International Journal of Machine Tools & Manufacture 159 (2020) 103626

Contents lists available at ScienceDirect

International Journal of Machine Tools and Manufacture

journal homepage: http://www.elsevier.com/locate/ijmactool

Effects of cyclic loading on subsurface microstructural changes of zirconia polycrystals in nanoscale mechanical processing

Koji Kosai, Jiwang Yan *

Department of Mechanical Engineering, Faculty of Science and Technology, Keio University, 3-14-1 Hiyoshi, Kohoku-ku, Yokohama, 223-8522, Japan

ARTICLE INFO

Keywords:
Cyclic load
Nanoindentation
Microstructural change
Phase transformation
Subsurface damage
Zirconia ceramics

ABSTRACT

Yttria stabilized zirconia (YSZ) is an attractive biomaterial with excellent properties, but its deformation mechanism under repetitive loads is still unclear. In this study, the subsurface microstructural changes of YSZ polycrystals under repetitive loading/unloading were investigated by multi-cyclic nanoindentation. Raman spectroscopy analysis revealed that a tetragonal-to-monoclinic (t-m) phase transformation occurred, and multi-cyclic indentation promoted this transformation significantly. Cross-sectional scanning transmission electron microscopy showed that monoclinic variants were extensively generated beneath the free surfaces outside the indent planes, whereas grain refinement was dominant beneath the indenter tip. In addition, load-displacement curve analysis demonstrated that the t-m phase transformation occurred during unloading rather than loading, and that the phase transformation-induced volume expansion caused an incremental change of residual indent depth. The extension of monoclinic variants was promoted by repetitive shear deformation, resulting in significant pileups, as detected by atomic force microscopy. The effect of sample surface preprocessing on indentation behaviors was also investigated. Microcracking and surface spalling were confirmed around the multi-cyclic indents made on a diamond-turned YSZ sample. Based on the experimental results, a model of subsurface microstructure distribution and evolution was established. The findings from this study help clarify the historical effects in subsurface damaging mechanism of brittle polycrystalline materials caused by cyclic tool-workpiece interactions in nanoscale mechanical processing.

1. Introduction

Zirconia is an important ceramic material having great potential of use in dental and biomedical applications, and so on. It exhibits different phases and mechanical properties by using different dopants. Yttria stabilized zirconia (YSZ) demonstrates a tetragonal-to-monoclinic (t-m) phase transformation under high stresses around crack tips [1,2]. As the density of a monoclinic phase is ~6% smaller than that of a tetragonal phase [3], the t-m phase transformation causes a volume expansion around the crack tip, which restricts further crack propagation and results in an increase in mechanical strength [4]. This characteristic enables YSZ to possess excellent material properties against mechanical/thermal shocks and abrasive erosions, but at the same time, leads to very poor machinability in various mechanical processes such as cutting, grinding, lapping and polishing. To prevent machining-induced surface/subsurface damages and improve the strength and service life of YSZ products, the investigation of mechanical load-induced microstructural changes, such as phase transformation and grain size change as well as their effects on mechanical properties of the material, is essential [5].

The t-m phase transformation is induced by shear stresses, as confirmed in experiments [6] and simulations [7]. The shear strain for t-m phase transformation is ~0.16, distinctly larger than that of the dilatational strain (~0.04) [7]. The transformation exhibits a twinning structure along a specific crystal plane to accommodate the shear strains [8,9]. In order to investigate the stress-induced phase transformation behaviors in YSZ, nanoindentation is a powerful tool. Nanoindentation provides information on various mechanical responses of materials induced by external forces, which are essential for material deformation mechanism analysis in micro/nanoscale. For examples, the t-m phase transformation occurs around an indented surface as confirmed in indentations at maximum loads of 630 mN [10], ~98 N [11], and 300 N [12] and such phase transformation affects the local mechanical properties [13]. At a maximum load of 150 N, the depth of t-m phase transformation region beneath the indent tip is ~6 times larger than that of the residual indent [14] and there is a clear relationship between the

* Corresponding author.
E-mail address: yan@mech.keio.ac.jp (J. Yan).

https://doi.org/10.1016/j.ijmachtools.2020.103626
Received 30 June 2020; Received in revised form 13 September 2020; Accepted 14 September 2020
Available online 18 September 2020

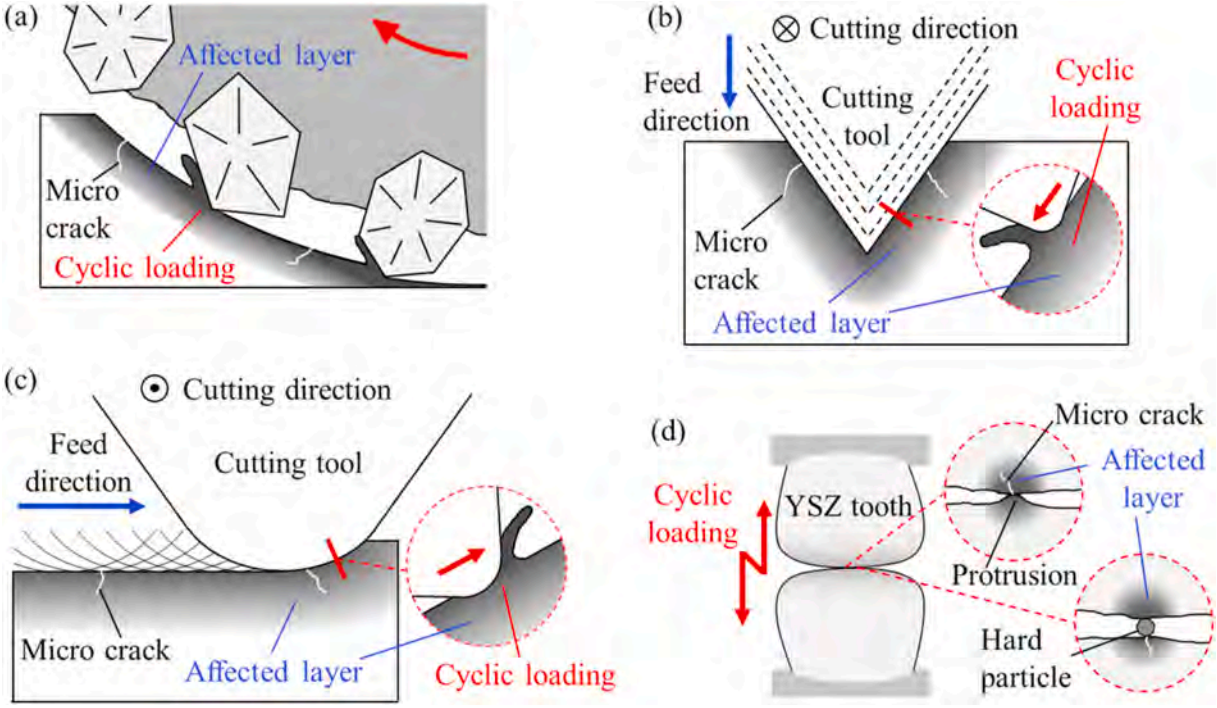

Fig. 1. Cyclic loading/unloading in machining processes and dental applications: (a) grinding; (b) grooving; (c) diamond turning; (d) tooth contact with microscopic protrusions and sandwiched hard particles.

Table 1
Major material properties.

Material properties	Values
Y_2O_3 [mol%]	3
Hardness [GPa]	12.5
Young's modulus [GPa]	210
Fracture toughness [$MPam^{1/2}$]	6.0

deep-region monoclinic phase and the material mechanical responses [15]. Indentation is an isothermal process; thus thermal effects need not to be considered. Moreover, it is possible to continuously record the real-time dynamic responses of the t-m phase transformation during loading and unloading. Continuous measurement of elastic modulus change during an indentation cycle enabled to monitor the evolution progress of the t-m phase transformation [16].

Zirconia can be machined by various methods. Grinding (Fig. 1 (a)) is commonly used for shaping teeth in dental applications [17]. Grooving by cutting tools (Fig. 1 (b)) [18] is used for fabricating zirconia optical fiber connecters. Moreover, to create aspherical or freeform 3D features, diamond turning (Fig. 1 (c)) or end milling are used [5]. The machinability and machining mechanisms should be investigated because they directly influence the surface integrity, mechanical properties and reliability of the machined workpiece [5,17]. In such nanoscale machining

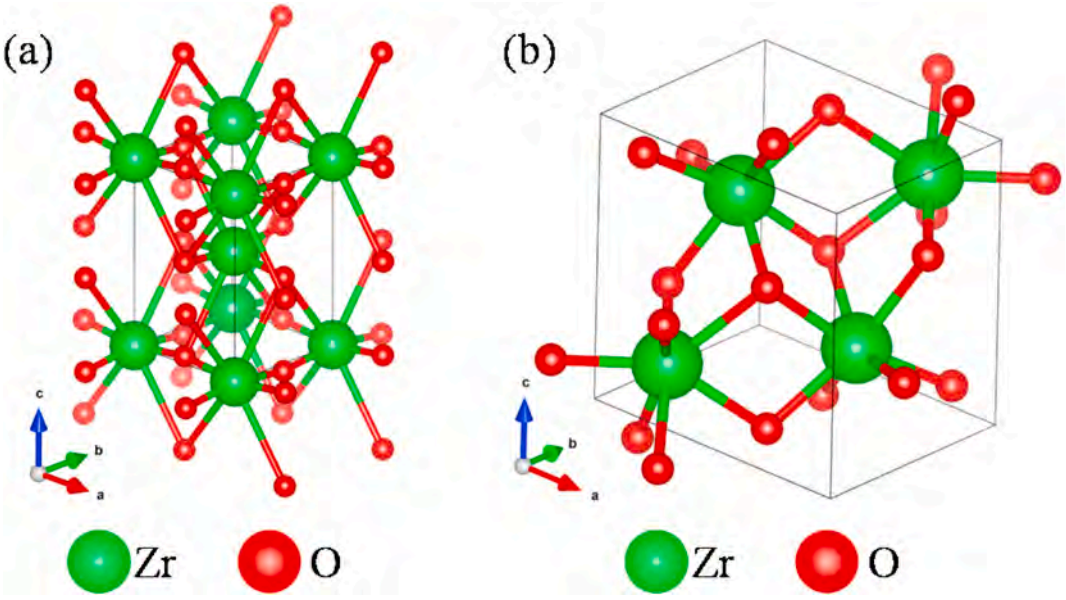

Fig. 2. Crystal structures of zirconia: (a) tetragonal phase; (b) monoclinic phase (drawn by VESTA [33]).

Table 2
Cutting conditions.

Cutting parameters	Values
Feed rate [μm/rev]	0.5
Depth of cut [μm]	5
Spindle rotation rate [rpm]	161–177
Cutting speed [m/min]	50
Cutting tool	
Tool material	Single-crystal diamond
Nose radius [mm]	1.0
Rake angle [°]	0
Relief angle [°]	8
Cutting atmosphere	Dry

processes, however, it is difficult to measure precisely the relationship among machining depth, force loading/unloading, material deformation and fracture in real time because they are high-speed dynamic processes with heat generation and tool wear. Another feature of these machining processes is that the workpiece is always under repetitive loads. The workpiece surface is always finished by multiple tool passes with repetitive tool-workpiece interactions involving periodic or non-periodic loading/unloading. In particular, in ultraprecision machining, the machining-affected layer becomes a few times thicker than the depth of material removal, as confirmed for silicon [19] and zirconia [5]. In this case, the machining-affected layer is cyclically machined for multiple times before being removed, as shown in Fig. 1 (a)–(c). Thus, the subsequent tool passes always alter the microstructures and properties of the affected layers formed in the previous tool passes, and the material responses to cyclic loading/unloading are very important for clarifying the machining mechanisms. However, it is extremely difficult to observe these material responses in real time for an actual machining process.

Moreover, in dental applications, external loads are acted on YSZ teeth in a highly repetitive manner, as shown in Fig. 1 (d). The surface of an artificial tooth is not completely flat but contains microscopic protrusions with affected layers. Sometimes, small hard particles like sands may be sandwiched in the gap and induce microscopic damages to the teeth. Thus, the understanding of material responses due to cyclic loads is of great importance for clarifying the subsurface damage and wear mechanism of artificial teeth. However, it is technologically difficult to observe such material responses in situ and in real time.

Nanoindentation can eliminate the effects of dynamic errors, heat generation, and changes in contact geometry due to surface wear, so that the relationship between loads and material responses can be observed more accurately. In addition, although the indenter shape is not completely the same as those of cutting tools, abrasive grains, and tooth

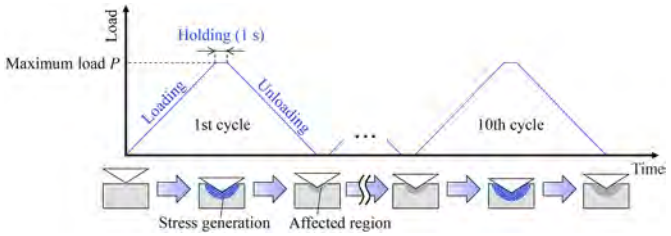

Fig. 4. Schematic of multi-cyclic nanoindentation and control graph of indentation load.

Table 3
Indentation conditions.

Indentation parameters	Values
Maximum load *P* [mN]	50, 1000
Loading/unloading rate [mN/s]	1
Indentation mode	Single, multi-cyclic (10 cycles)
Indenter geometry	Berkovich
Indenter material	Single-crystal diamond

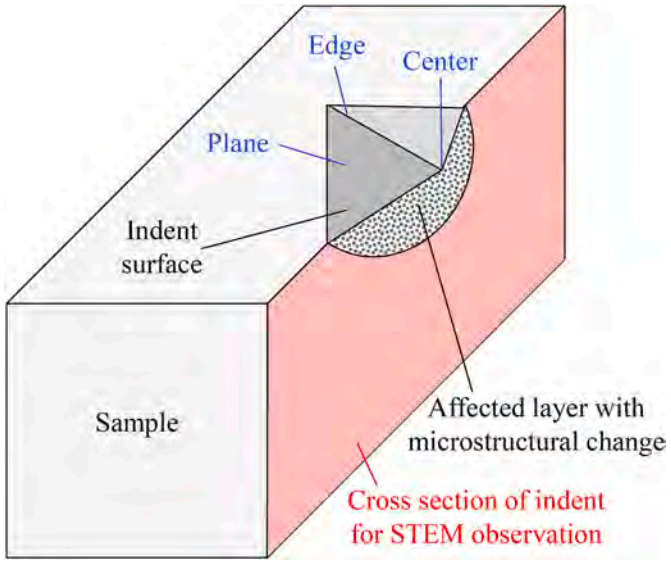

Fig. 5. Indication of spots analyzed by Raman spectroscopy and cross section observed by STEM.

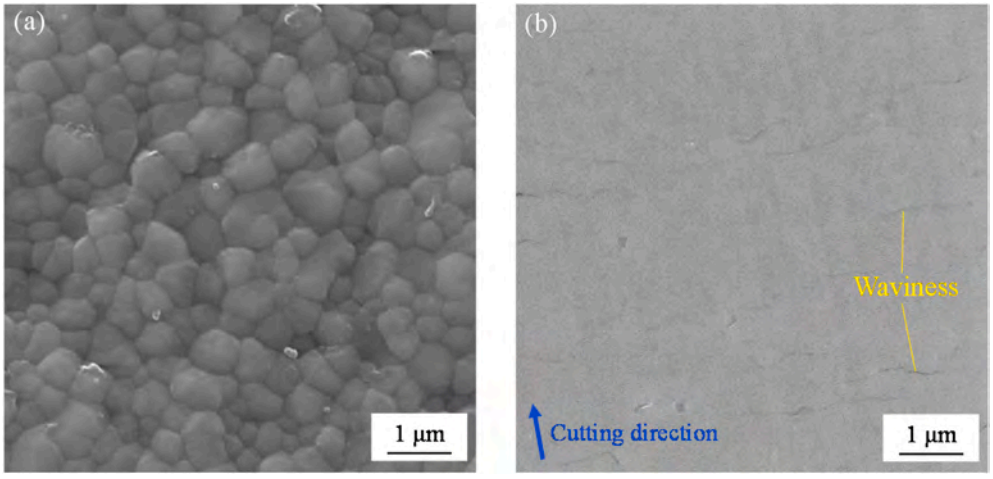

Fig. 3. SEM images of (a) unmachined and (b) diamond-turned surfaces before indentation tests.

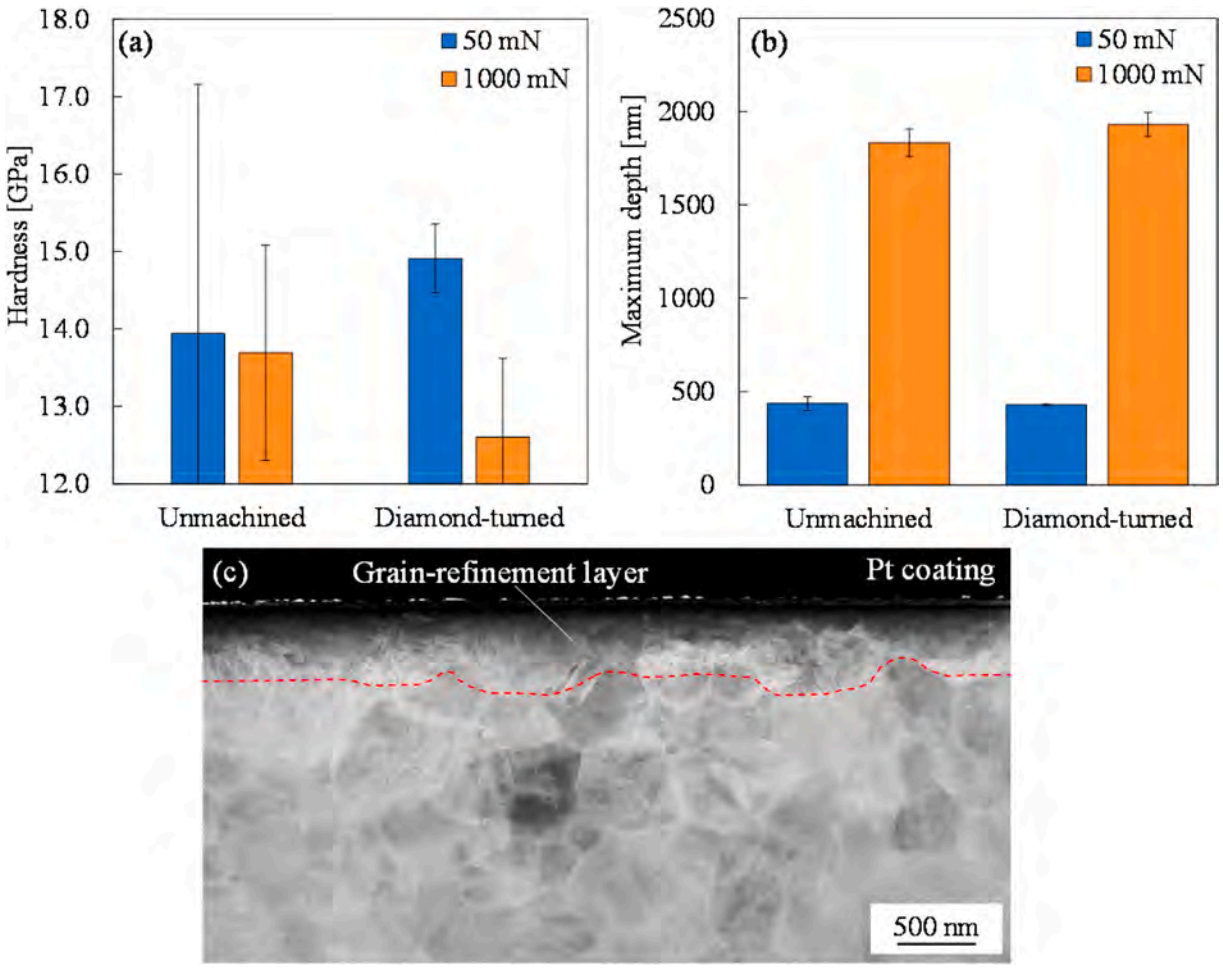

Fig. 6. (a) Microhardness and (b) maximum indentation depth at single indentations of each surface; (c) cross-sectional STEM photograph of the diamond-turned sample.

surface protrusions, the basic contact geometries are similar. Thus, the indentation results provide generic knowledge of nanoscale contact mechanics and material structural changes which is useful for clarifying the ultraprecision machining phenomenon and investigating the effects of depth of cut [20,21] on ductile-brittle transition [22] in grinding, and material removal in ultrasonic vibration assisted side grinding [23,24], as well as tooth wear/damage mechanisms.

However, up to now, to the best of the author's knowledge, only single indentation was employed for phase transformation analysis of YSZ, while the effects of repetitive loading/unloading have never been investigated. To narrow the gap and clarify the mechanical responses of YSZ under repetitive load/unloading, multi-cyclic nanoindentation tests will be performed in this study. Multi-cyclic nanoindentation has been attempted for investigating the microstructural changes of various materials, and multi-cyclic loading/unloading was found to cause distinctly different, and even reverse, effects on accumulating/releasing strains, hardening/softening surface layers, closing/opening cracks, and so on. For example, multi-cyclic indentation greatly changes phase transformation and deformation behaviors beneath the indents of silicon [25,26] and germanium [27,28], but does not cause any phase transformation in gallium arsenide [29]. In addition, propagation of crystal defects in multi-cyclic nanoindentation were reported in germanium [28], iron [30], and stainless steel [31].

From this point of view, multi-cyclic indentation tests may also provide insights into nanoscale material deformation behavior and subsurface damage formation mechanism of YSZ under cyclic loading/unloading, which is important for clarifying the mechanisms of ultraprecision machining processes and tooth damage/wear in dental applications. By multi-cyclic nanoindentation, micro/nanoscale material behaviors under cyclic load can be investigated in a simple and fast way, which gives different knowledge from general fatigue tests [32] where far more cycles of loading/unloading are required.

In this study, multi-cyclic nanoindentation tests were performed on YSZ polycrystals with different surface finishes under various conditions. The subsurface microstructural changes, including phase transformation and grain size change and deformation, were investigated in detail by using various characterization methods such as Raman spectroscopy, scanning electron microscopy (SEM), atomic force microscopy (AFM) and scanning transmission electron microscopy (STEM). In addition, the load-displacement curve and contact pressure were analyzed to characterize the occurrence stage of phase transformation. Based on the experimental results, the mechanisms of phase transformation and grain size change under cyclic loading/unloading were discussed and compared with those of single indentations. It is expected that the findings in this study will narrow the gap in the understanding of cyclic load-induced subsurface damaging behaviors of YSZ and other hard brittle polycrystalline materials.

2. Material and methods

2.1. Material

A YSZ polycrystal with 3 mol% yttria concentration produced by Tosoh Corporation, Japan was used as a sample. Table 1 gives the major

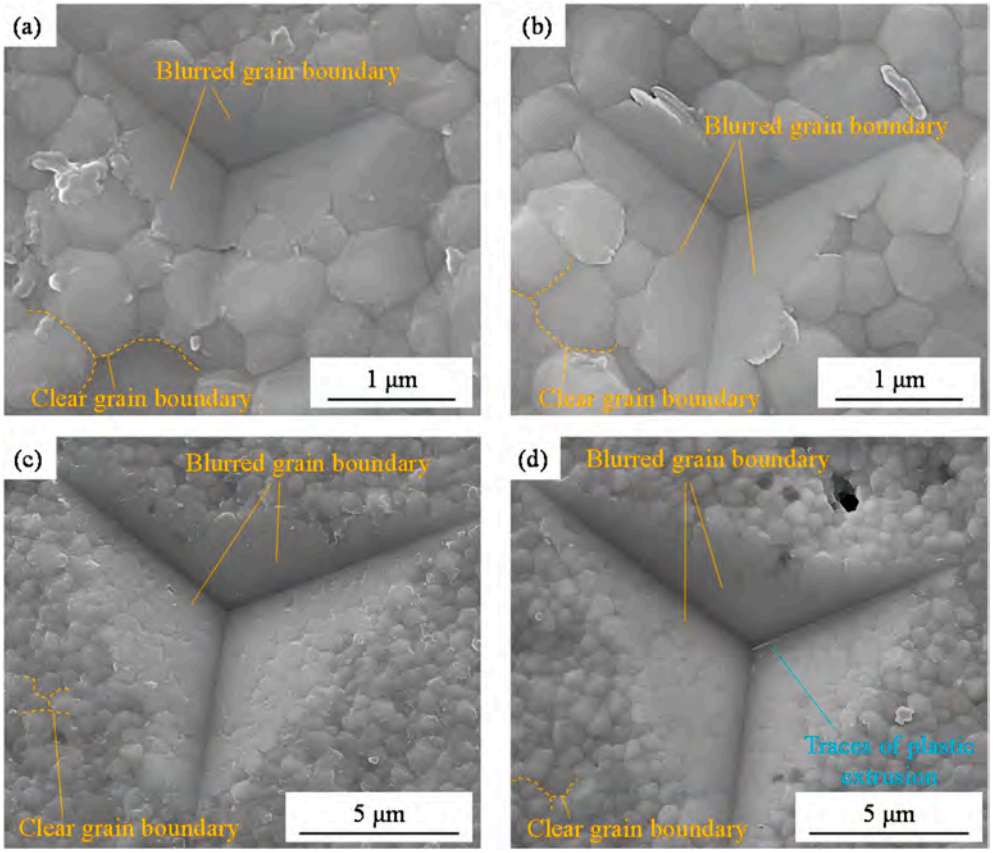

Fig. 7. SEM images of indents on the unmachined surface: (a) 50 mN, single; (b) 50 mN, multi-cyclic; (c) 1000 mN, single; (d) 1000 mN, multi-cyclic.

material properties provided by the manufacturer. At room temperature, YSZ has a tetragonal phase, as shown in Fig. 2 (a) (figure drawn by VESTA [33]). In sample preparation processes such as slicing and polishing, a layer of material may change to a monoclinic phase as shown in Fig. 2 (b). In this study, the layer of monoclinic phase was changed back to the original tetragonal phase by performing heat-treatment of the samples at 1300 °C for 1 h. Therefore, all the samples used in this study started from a tetragonal phase.

Two types of sample surfaces were used for nanoindentation experiments: a heat-treated surface without machining, and an ultraprecision diamond-turned surface. The diamond-turned sample was prepared using an ultraprecision lathe ASP-15 (Nachi-Fujikoshi Corp., Japan) under the conditions shown in Table 2. It was confirmed that a nanometric smooth surface could be obtained under such cutting conditions [5]. Fig. 3 shows SEM images of both unmachined and diamond-turned surfaces. The unmachined surface is rough with crystal grains clearly seen, whereas the diamond-turned surface is very smooth without identifiable grain boundaries. The small waviness on the diamond-turned surface might be a result of small-amplitude chattering during the cutting process. After diamond turning, the surface roughness measured by a white light interferometer over 20 μm squares was reduced from 51 nm Sa to 5 nm Sa. In diamond turning, a thin subsurface damage layer will be generated [5], which might affect the subsequent machining characteristics. By performing nanoindentation on the diamond-turned surface, the effect of preexisting defects on the nanoindentation behavior of YSZ can be identified, which is important for understanding subsurface damaging behaviors in ultraprecision cutting.

2.2. Nanoindentation system

Indentation tests were performed by using a single-crystal diamond Berkovich indenter equipped on a nanoindentation instrument ENT-1100a (Elionix Inc., Japan). Fig. 4 shows a schematic diagram of multi-cyclic indentation and the control graph of the indentation load. In each single indentation, the indenter was loaded at a constant rate before the maximum load was reached, held for 1 s, and then unloaded at the same rate as loading. During multi-cyclic indentation, the situation of stress generation and the resulting subsurface microstructures will change with the cycle number, as schematically illustrated in the diagram of Fig. 4. These changes will be investigated in this study. Table 3 shows the indentation conditions. For creating large indents enough for clearly distinguishing each region of an indent in phase characterization as explained in Section 2.3, the maximum load was set to 1000 mN, which led to a micron-level indentation depth. For comparison, indentation at a maximum load of 50 mN was also performed, which caused a submicron-level indentation depth. For a high loading/unloading rate, phase transformation starting on loading with fast strain rates may not complete in the loading process but continues to the unloading or subsequent cycles [16]. In this study, to prevent continuation of such phase transformation to the subsequent indentation cycles and independently analyze the phase transformation behaviors for each loading/unloading step, a slow loading/unloading rate of 1 mN/s was selected.

In the multi-cyclic indentation mode, the above-mentioned indentation step was repeated 10 times on the same point. For each condition, 5 sets of indentation tests were performed on different points to confirm repeatability. On the diamond-turned samples, the indentation points were carefully located by CCD camera observation in order not to overlap with preexisting surface defects formed by the diamond turning process.

2.3. Characterization methods

The indented surfaces were observed by SEM and AFM to confirm the

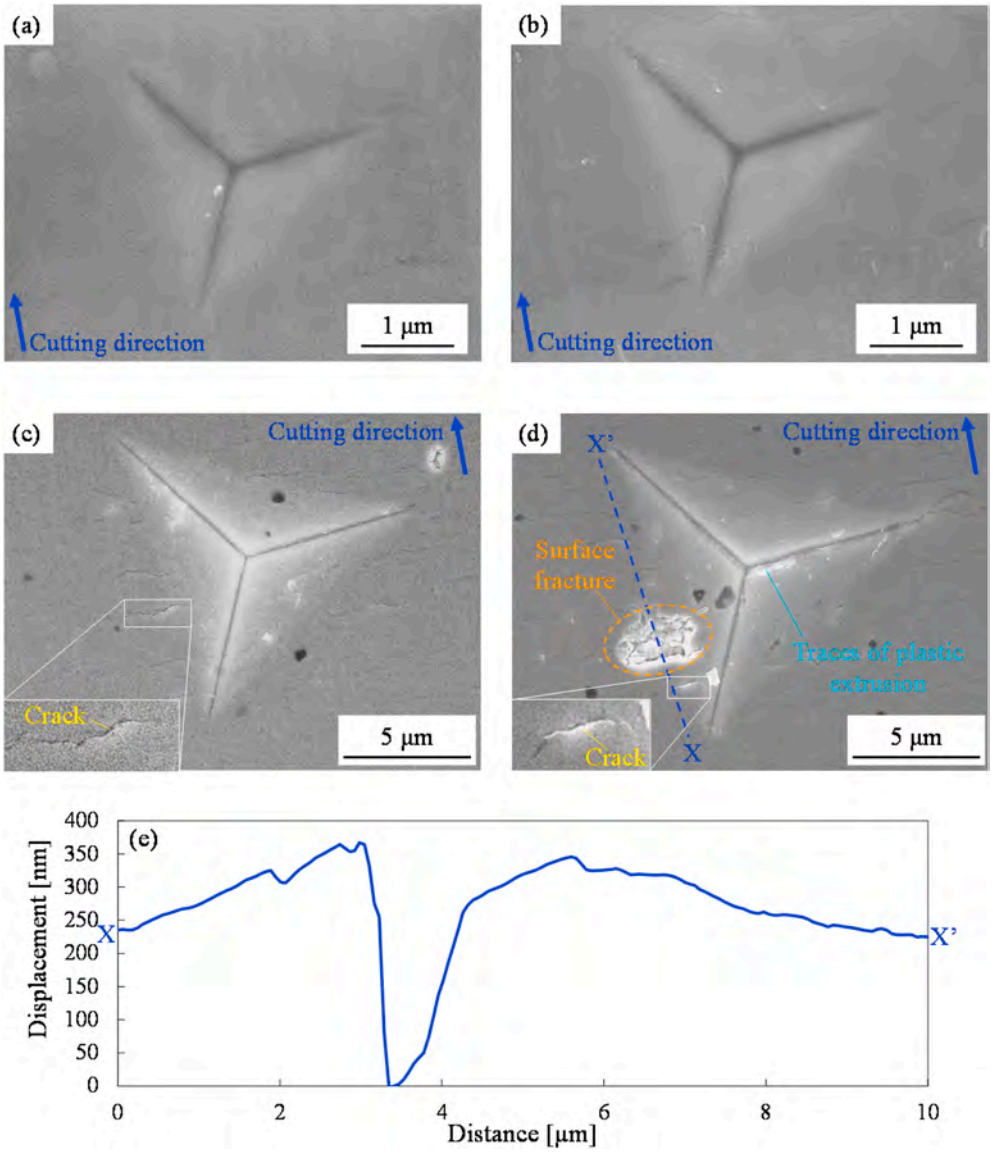

Fig. 8. SEM images of indents on the diamond-turned surface: (a) 50 mN, single; (b) 50 mN, multi-cyclic; (c) 1000 mN, single; (d) 1000 mN, multi-cyclic; (e) cross-sectional profile of X-X' in (d).

deformation of the material after indentation. Then, the surfaces were investigated by a laser micro-Raman spectrometer inVia (Renishaw plc., UK) with 532 nm laser wavelength and ~1 μm laser spot size. In laser Raman spectroscopy, the noise level depends on the incident laser intensity. To reduce noise in the Raman spectra, in this study, the laser beam was irradiated on the samples without attenuating its intensity, although such attenuation is usually used for protecting sensitive materials in Raman measurements. On the other hand, too strong laser irradiation may induce further phase transformation of the sample. In this experiment, we confirmed that the Raman spectra were not changed in repetitive Raman measurements at the same spot. Therefore, the laser irradiation did not induce further phase transformation. The center, plane and edge of an indent at a maximum load of 1000 mN were respectively investigated, as illustrated in Fig. 5. For quantitative evaluation of t-m phase transformation, the monoclinic volume ratio V_m was calculated by using the following equation [34]:

$$V_m = \frac{I_m^{181} + I_m^{190}}{2.07 I_t^{147} + I_m^{181} + I_m^{190}} \quad (1)$$

where I_m^k is the integrated intensity at a wavenumber of k corresponding to a monoclinic phase, and I_t^k is the integrated intensity corresponding to a tetragonal phase. By comparing the monoclinic volume ratios, phase transformation behaviors can be quantitatively analyzed. In addition, the cross section indicated in Fig. 5 was observed by STEM to observe the subsurface microstructures. The cross-sectional samples for STEM observation were prepared and thinned by a focused ion beam (FIB) system to a thickness of ~100 nm after coating the surface by Pt for protection. The STEM observation was performed at a voltage of 200 kV. Moreover, deformation behaviors during loading/unloading processes were investigated by analyzing the load-displacement curves and average contact pressures.

3. Results and discussion

3.1. Microhardness change in surface layer

Fig. 6 (a) is the microhardness of unmachined and diamond-turned surfaces measured by single indentations at two levels of maximum loads: 50 mN and 1000 mN. At 50 mN, the microhardness of the diamond-turned surface is ~1.0 GPa higher than that of the unmachined

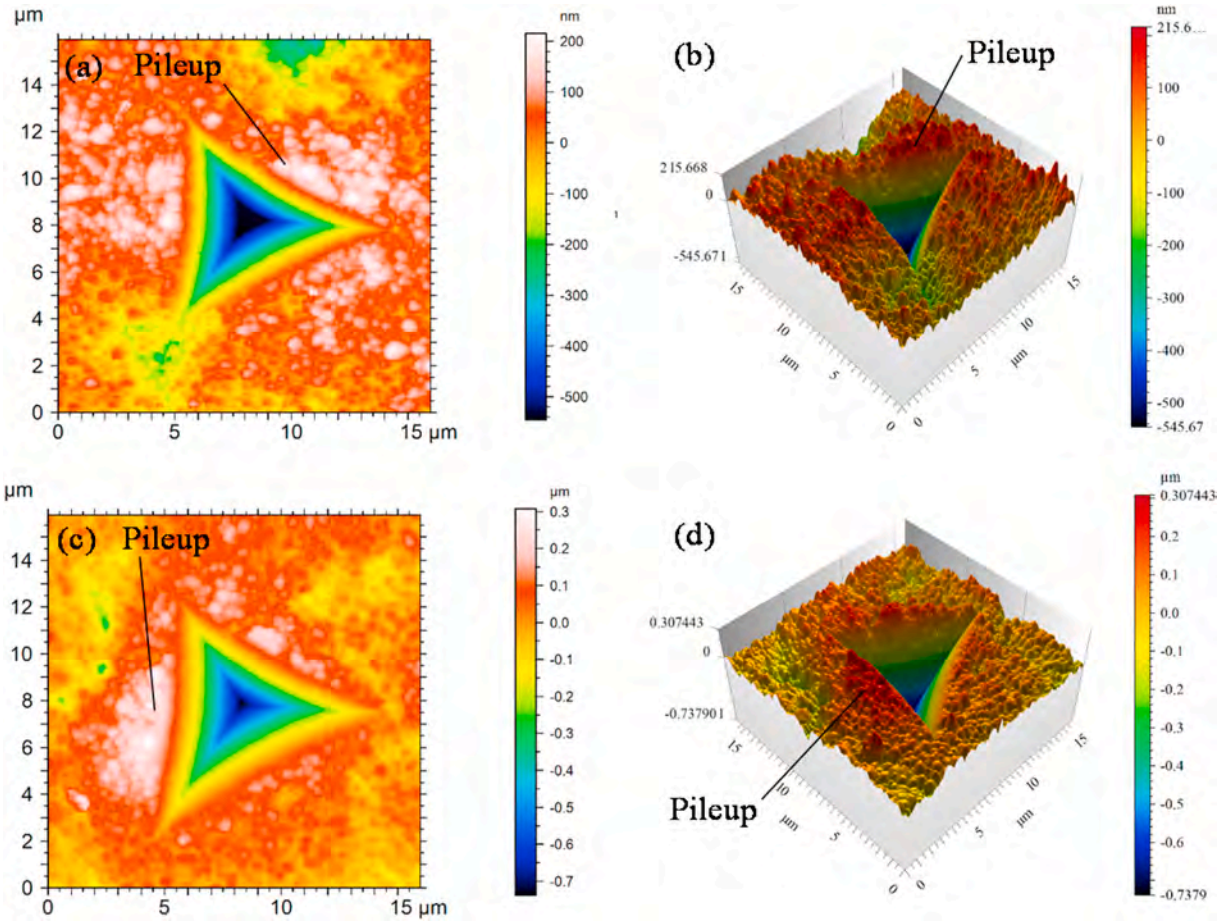

Fig. 9. Typical surface topographies of indents at 1000 mN on the unmachined surface: (a) single, 2D; (b) single, 3D; (c) multi-cyclic, 2D; (d) multi-cyclic, 3D.

surface. This is due to the presence of a grain-refinement layer formed in the cutting process. Fig. 6 (c) is a cross-sectional STEM photograph of the diamond-turned sample, where a grain-refinement layer, the thickness of which is ~500 nm, is generated beneath the surface. The grain-refinement layer thickness is very close to the maximum indentation depth (~430 nm), as can be seen in Fig. 6 (b), so that the indentation is done inside the grain refinement layer in this case. It is known that YSZ exhibits higher hardness with the reduction of the grain size [35]. Thus, it is the grain-refinement layer that increased the microhardness. In addition, the high pressure during ultraprecision cutting process may increase the density of the nano- and submicron-grained YSZ, which in turn causes a hardness increase [36]. It is noteworthy that at 1000 mN, the microhardness of the diamond-turned surface is ~1.1 GPa lower than that of the unmachined surface. This might be caused by the indentation-induced microcracking of the grain-refinement layer observed in Fig. 8 (c), since the opening of microcracks increases the contact area between the indenter and sample [37]. From this point of view, the precutting-induced hardened surface layer may affect the multi-cycle indentation behaviors.

Note that in indentation at 50 mN on the unmachined surface, the error range of hardness measurement became significantly larger than those of other conditions. At this indentation load, the indent size was so small that it is comparable with the grain size of YSZ, as shown in SEM observation (Fig. 7 (a)) in Section 3.2. Therefore, the indentation process was significantly affected by the surface unevenness and crystallographic anisotropy of the exposed grains, resulting in more varied hardness than indentation at 1000 mN. For the diamond-turned surface, however, the surface was flattened and the grains in the surface layer were refined, thus the hardness measurement was reliable.

3.2. Indent surface morphology

Fig. 7 presents SEM images of the indented unmachined surface at single and multi-cyclic indentations with different maximum loads. The indents are generally smooth without brittle fractures for both single and multi-cyclic indentations. On the raw surfaces around indented planes, grain boundaries are clearly seen, although grain boundaries become blurred near the indent centers and edges, especially at a maximum load of 1000 mN, as shown in Fig. 7 (c) and (d). These results indicate significant plastic deformation of the crystal grains due to the pressing of the indenter faces.

The SEM images of the diamond-turned surface are shown in Fig. 8. Though the indents in Fig. 8 (a) and (b) are smooth without any fractures, the indents obtained at 1000 mN showed cracks around the indent (Fig. 8 (c) and (d)). The cracks were formed along the waviness observed on the diamond-turned surface in Fig. 3 (b). In addition, multi-cyclic indentation induced surface fracture at the indent shown in Fig. 8 (d). Fig. 8 (e) is a cross-sectional profile of the line X-X' in Fig. 8 (d) measured by AFM. The depth of the surface fracture is ~350 nm, which is close to the thickness of the grain-refinement layer in Fig. 6 (c). Hence, the surface fracture might have been caused by the spalling of the grain-refinement layer. It is considered that cyclic indentation at a high load induced microcracks along the interface between the grain-refinement layer and the bulk. Then the microcracks propagate and result in spalling of the grain-refinement layer.

In single indentations, plastic flows occur beneath the indent surfaces or outside the indents as pileups. In this study, however, the SEM images showed clear traces of plastic extrusions out of the surface inside the indents in multi-cyclic indentation (Fig. 7 (d) and Fig. 8 (d)). This kind of extrusion has never been found for single indentations.

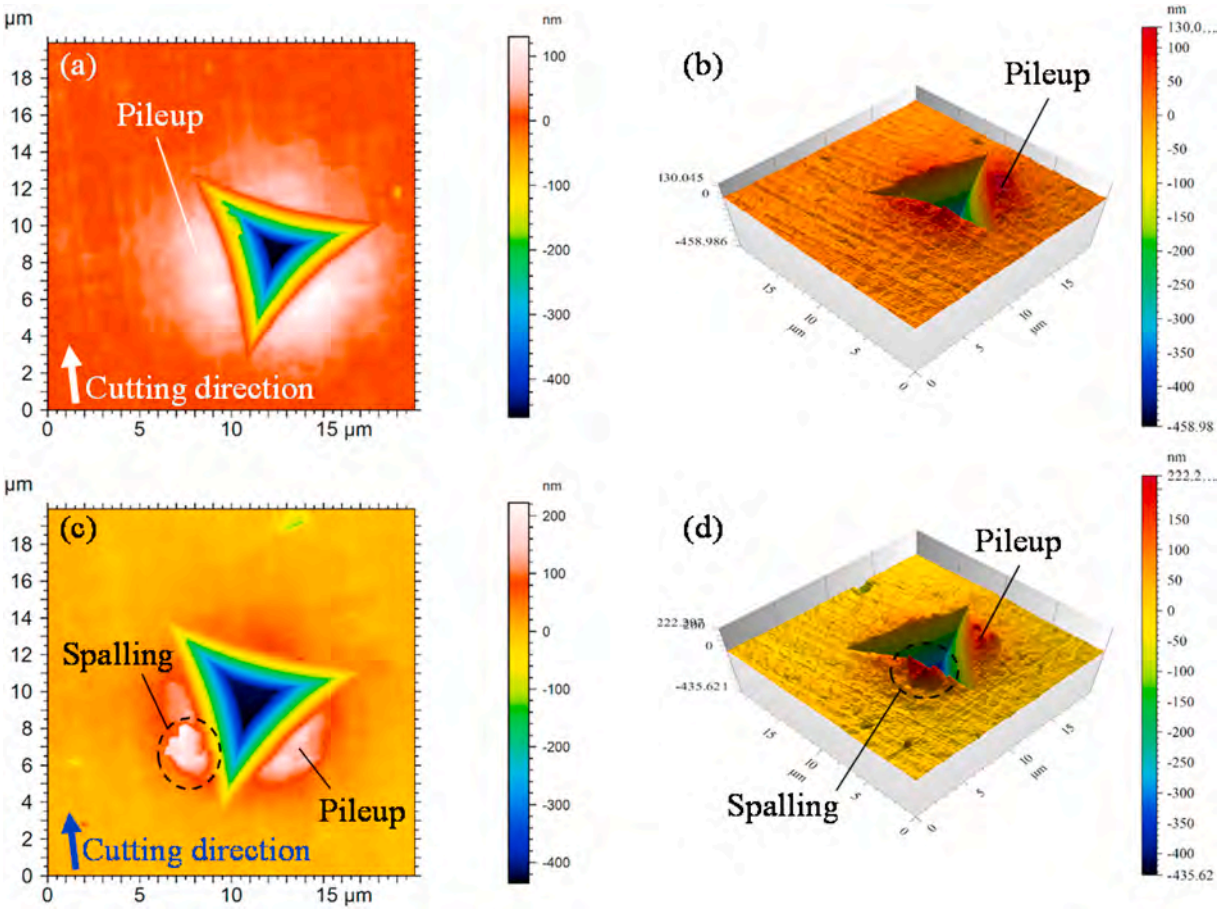

Fig. 10. Typical surface topographies of indents at 1000 mN on the diamond-turned surface: (a) single, 2D; (b) single, 3D; (c) multi-cyclic, 2D; (d) multi-cyclic, 3D.

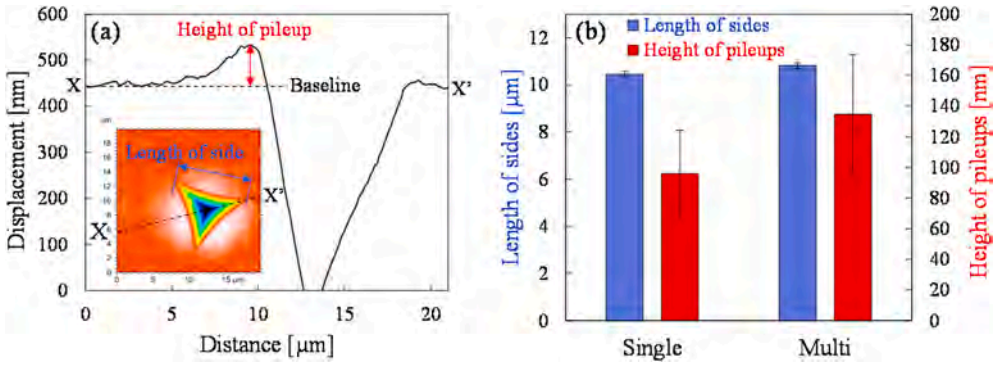

Fig. 11. (a) Cross-sectional profile for explaining the length of side and height of pileup; (b) comparison of the length of sides and height of pileups.

Therefore, multi-cyclic indentations should have promoted the local plastic flow along the indent surface due to cyclic shear stress generated at the interface of the indenter and the workpiece material. The surface plastic extrusion phenomenon observed in this study indicates that surface roughening may occur in a machining process with multiple tool passes. That is to say, subsequent tool passes may deteriorate a smooth surface achieved by previous cuts, rather than improving the surface quality.

3.3. Indent size and surface pileup comparison

For quantitative analysis of the surface topography, the indented surfaces were precisely measured by AFM. Fig. 9 and Fig. 10 show typical 2D and 3D topographies of indents at 1000 mN on the unmachined and diamond-turned surfaces measured by AFM. In Fig. 9, despite of significant surface roughness, pileups can be identified around the indents. The pileups of multi-cyclic indentations are bigger than those of single indentations. In Fig. 10, pileups can be more clearly identified around the indent planes, as well as spalling in multi-cyclic indentation (Fig. 10 (c) and (d)). The asymmetry of the pileups at each side would be due to imperfect perpendicular orientation of indentation to the sample surface. Such asymmetry is often observed in indentation as deviation of shear bands [38,39]. In addition, anisotropy of the surface property due to the cutting direction may also affect the result. Fig. 11 is comparison of the length of indent sides and height of pileups. The baseline was set at the minimum height of the adjacent flat surface. Multi-cyclic indentations slightly expanded the indents and produced pileups which were ~39 nm higher than those of single

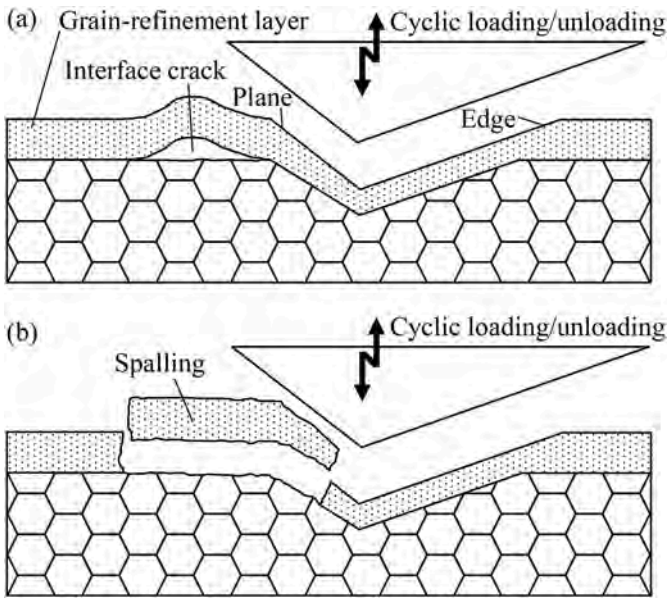

Fig. 12. Different sizes of spalling: (a) spalling remaining on the surface with an uplift, (b) spalling with complete removal of grain-refinement layer.

indentations. As the surface pileups are formed by side flow of the material and volume expansion due to the t-m phase transformation [10, 12], the higher surface pileups indicate that multi-cyclic indentation promoted the material flow and phase transformation.

In the AFM measurement results of Fig. 10 (c) and (d), the spall of the grain-refinement layer remained on the surface with an uplift, while the indent plane was flat. Therefore, spalling was limited in the surrounding area of the indent and the spall was not completely removed. In contrast, the spalling shown in Fig. 8 (d) was more extensive, resulting in complete removal of the grain-refinement layer over a large area including a part of the indent plane. These two kinds of spalling phenomena were typically observed in multi-cyclic indentations, while no spalling was found in single indentations. From this fact, it is presumable that multi-cyclic loading/unloading promotes the crack initiation and propagation along the boundary between the grain-refinement layer and the bulk, as schematically illustrated in Fig. 12 (a). The boundary becomes weaker than the bulk due to the mismatch of crystal lattices. The size of spalling depends on the location of indent and the distribution of preexisting defects in the surface layer caused by diamond turning. If there are a large amount of defects caused by diamond turning in the indented area, the crack propagation along the boundary of grain-refinement layer and bulk is promoted, which may result in large-area removal of the layer, as shown in Fig. 12 (b).

In this study, the samples prepared by diamond turning in a ductile mode were used for indentation tests, thus the effect of grain-refinement layer was dominant in the indentation tests. If the sample is prepared by diamond turning in a brittle mode [5], however, the cutting-induced cracks will affect the fracturing and spalling behavior in indentation tests. Similar phenomena might occur to the machined surfaces of other brittle polycrystalline materials such as ZnSe [40]. Furthermore, in grinding of YSZ and other ceramic materials, subsurface cracks occur significantly [41], thus it is presumable that cyclic indentation will promote the propagation of the grinding-induced cracks, leading to large scale surface fractures. Similar trends might be applicable for edge chipping phenomena in ultrasonic assisted grinding [42].

3.4. Phase transformation analysis

As the aforementioned indent surface morphology may be affected by phase transformations of the sample material, the phase changes after indentation were investigated by Raman spectroscopy. Fig. 13 shows the obtained Raman spectra of indents. The t-m phase transformation from the initial tetragonal phase to monoclinic phase was found on both unmachined and diamond-turned surfaces. The indentations caused formation of the monoclinic phase exhibiting Raman peaks around 180-190 cm^{-1}. In particular, Raman spectra obtained from indent planes exhibit stronger monoclinic peaks than those from edges and centers.

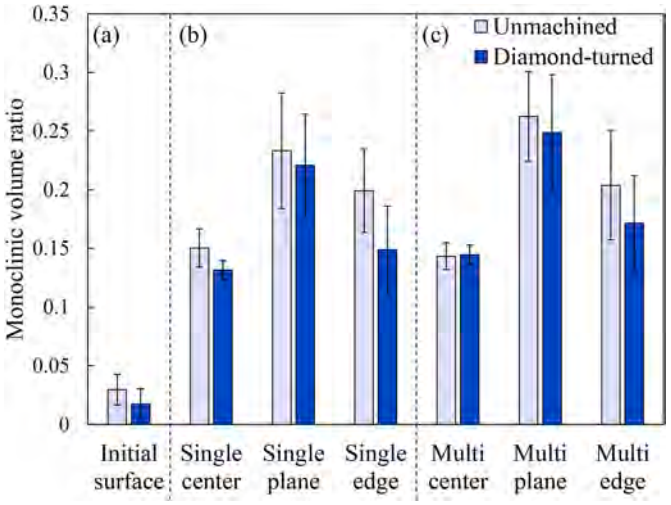

Fig. 14. Monoclinic volume ratios for each condition and position: (a) initial surface; (b) single and (c) multi-cyclic indentations.

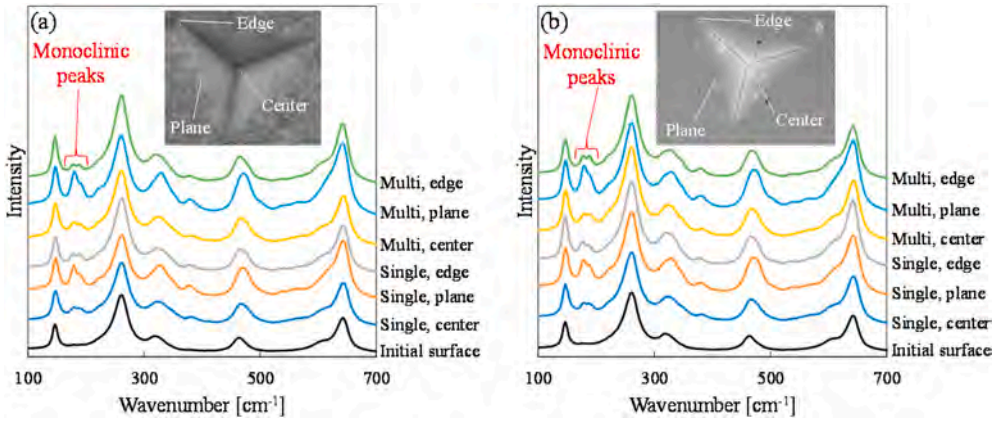

Fig. 13. Typical Raman spectra at each position of indents in both single and multi-cyclic indentations: (a) unmachined surface; (b) diamond-turned surface.

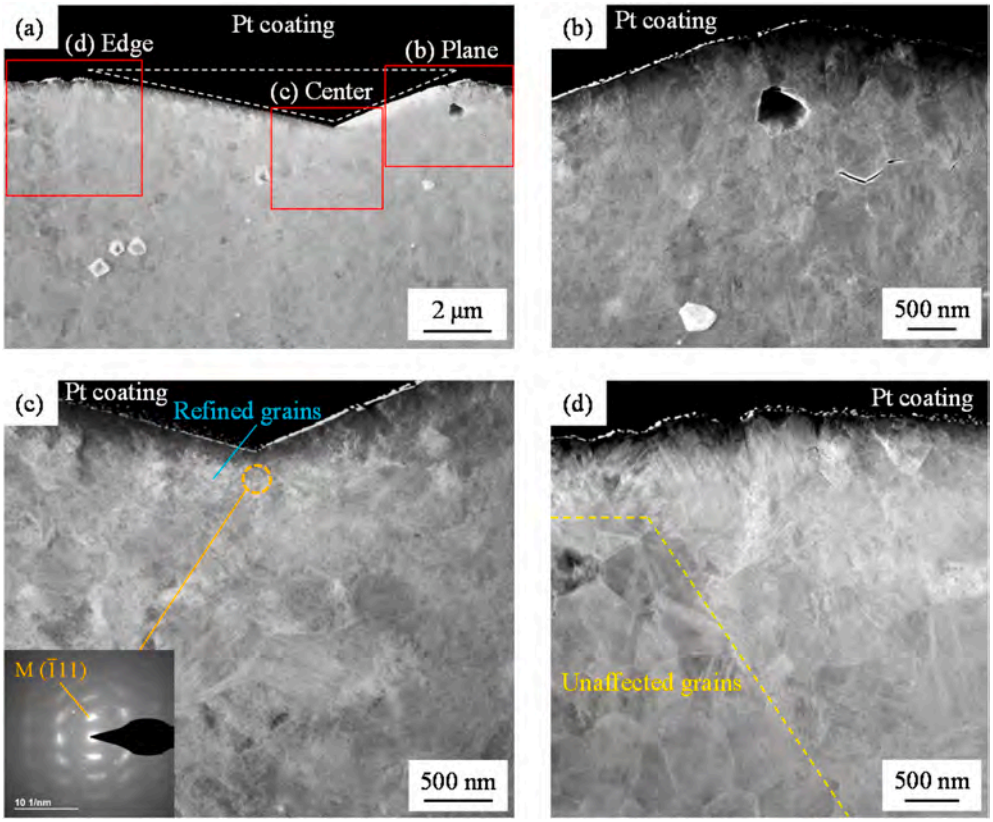

Fig. 15. Cross-sectional STEM images of single indentation at 1000 mN on the unmachined surface (M: monoclinic phase): (a) whole of the indent; (b) plane; (c) center; (d) edge.

From the Raman spectra, monoclinic volume ratios were calculated. Eq. (1) was used for the calculation, and the statistical result was presented in Fig. 14. In both single and multi-cyclic indentations, indentation processes significantly increased monoclinic volume ratios from those of initial surfaces. In particular, the indent planes showed the highest monoclinic volume ratios. The indent edges exhibited lower monoclinic volume ratios than indent planes, and the indent centers showed the lowest monoclinic volume ratios. In addition, multi-cyclic indentations demonstrate higher monoclinic volume ratios as compared to single indentations, indicating that repetitive loading/unloading promoted t-m phase transformation.

Comparing the unmachined and diamond-turned surfaces, the diamond-turned surface exhibited lower monoclinic volume ratios: ~5% lower at the planes, 16–25% lower at the edges. This is because cracks and fractures were formed around indents on the diamond-turned surface, which released the stress, and in turn, suppressed the t-m phase transformation. The second possible reason is that the residual compressive stress induced by the high pressure in cutting [5] restricts volume expansion and t-m phase transformation [43], which is experimentally confirmed in indentation of YSZ [14] and zirconia toughened alumina [44]. Another reason might be the effect of the grain-refinement layer generated by cutting. It is reported that finer-grained YSZ polycrystals show less t-m phase transformation during indentation tests [11]. Therefore, the grain-refinement layer might restrict t-m phase transformation as compared to the unmachined surface.

3.5. Cross-sectional STEM observation

Next, for investigating the indentation-induced subsurface structural changes of YSZ, the subsurface structures of single and multi-cyclic indents were observed by STEM. Cross sections of indents formed by single and multi-cyclic indentations on the unmachined surface at 1000 mN were observed as Fig. 15 and Fig. 16. As compared to Fig. 15 (b), parallel variants are extensively formed around the indent plane in Fig. 16 (b) and (e). The variants were formed by a monoclinic phase as demonstrated by selected area diffraction pattern (SADP) in Fig. 16 (e). In previous studies, similar variants formed by martensitic t-m phase transformation in subsurface were observed by TEM, and some variants propagate into the adjacent grains cross the grain boundaries, which is a result of monoclinic phase propagation [9,15]. These facts indicate that around the indent plane, monoclinic variants formation and propagation were promoted by multi-cyclic indentation, resulting in higher monoclinic volume ratios than other positions. This agrees well with the results shown in Fig. 14, demonstrating that in multi-cyclic indentation, the indent plane exhibits a ~29% higher monoclinic volume ratio than the edge, ~83% higher than the center on the unmachined surface.

It should be mentioned that most of the monoclinic variants are observed outside the indent (the right parts of Fig. 16 (b)) rather than beneath the indent. This result might be due to the difference in stress distribution. During loading, the Mises stress calculated by finite element method is estimated in excess of 2 GPa outside the indent plane [45]. It is also found through simulation that in indentation of ceramics, large compressive stresses in excess of 5 GPa is generated beneath the indenter, which is significantly different from the situation of the surrounding area near the free surface [46]. As known from previous researches, the t-m phase transformation is promoted by shear stress [47], whereas compressive stress suppresses t-m phase transformation by confining volume expansion [43]. Hence, t-m phase transformation occurs significantly in the stressed region outside the indent, whereas the transformation is suppressed by strong compression beneath the indenter. The monoclinic variants cause further stress at the grain boundaries, which induces further propagation of monoclinic variants to the adjacent grains [9]. By repeating this process, extensive monoclinic

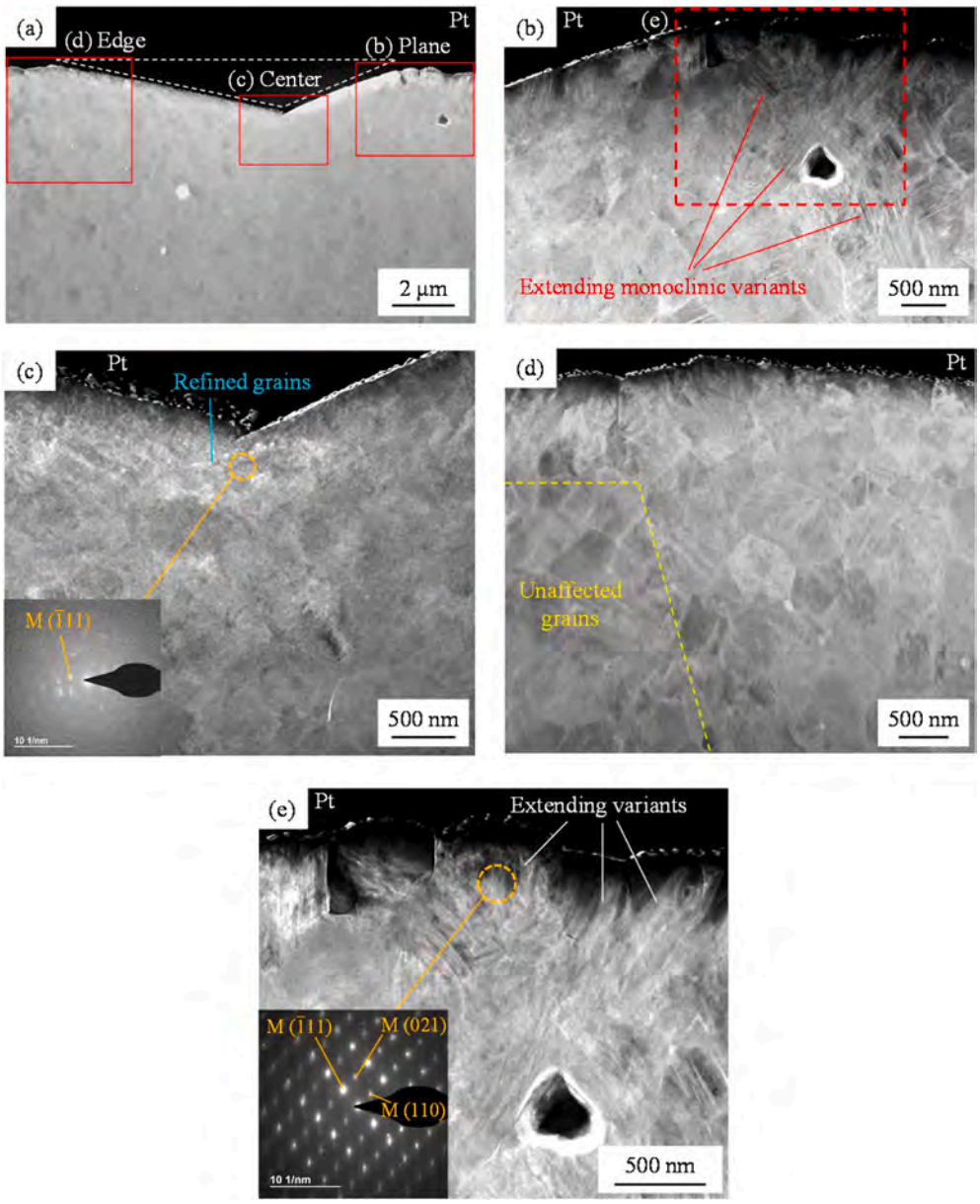

Fig. 16. Cross-sectional STEM images of multi-cyclic indentation at 1000 mN on the unmachined surface (M: monoclinic phase): (a) whole of the indent; (b) plane; (c) center; (d) edge; (e) enlarged view of the indent plane (b).

variants are generated even at the surface grains after multi-cyclic indentation, as observed in Fig. 16 (e).

The monoclinic variants extended to a depth of a few microns, which was far larger than the grain-refinement layer thickness (~500 nm, as confirmed in Fig. 6 (c)). Hence, it is expected that similar t-m phase transformation behaviors occurred beneath the grain-refinement layer of the diamond-turned surface in multi-cyclic indentation, resulting in a ~13% higher monoclinic volume ratio in multi-cyclic indentation than that of single indentation. This trend is the same as that of the unmachined surface where multi-cyclic indentation resulted in a ~13% higher monoclinic volume ratio than that of single indentation, as shown in Fig. 14.

Immediately beneath the indent centers in Figs. 15 (c) and Fig. 16 (c), boundaries of original grains become blurred and diminished, and circular SADPs were observed, indicating the occurrence of grain refinement. The traces of plastic extrusion in Figs. 7 (d) and Fig. 8 (d) might be a result of localized flow of the refined grains by repetitive loading/unloading. The existence of monoclinic phase is also confirmed in the SADP, which corresponds to the result of the monoclinic volume ratio. However, the indent centers exhibited lower ratios than the indent planes and edges as shown in Fig. 14. In the high pressure torsion experiment of YSZ, grain refinement by dislocation formation and propagation was reported [47]. Therefore, high shear stress with strong compression at the indent centers would preferentially promote dislocation formation and grain refinement, while t-m phase transformation was suppressed due to compressive stress [43]. This explains the lowest monoclinic volume ratios at the indent centers in Fig. 14.

Figs. 15 (d) and Fig. 16 (d) are the STEM images around the indent edges. Raw grain boundaries are clearly identified, indicating that microstructural change outside the indent is insignificant because grain boundaries become blurred due to contrast change by microstructural changes such as grain refinement, crystal defects, and phase transformation. For quantitative evaluation of the blurriness, contrast peak distribution in the STEM images were counted by using the ImageJ software. It should be noted that the number of contrast peaks easily fluctuates by changing image contrast, so it is meaningless to compare

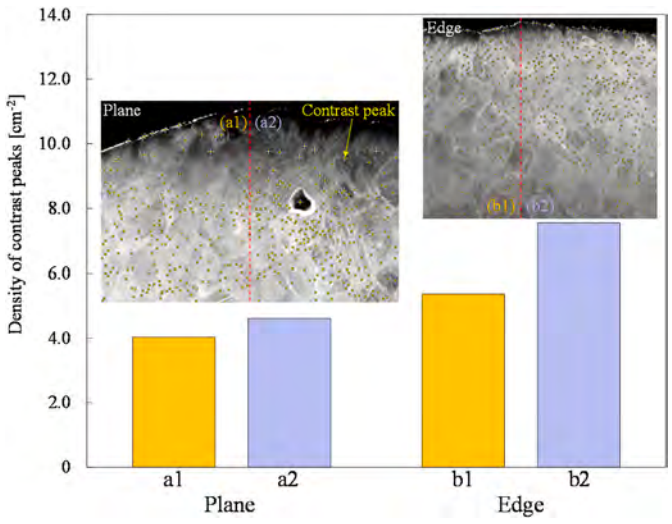

Fig. 17. Distributions and density of contrast peaks in STEM images of the indent plane and indent edge in Fig. 16 (contrast peaks on the boundaries between each region and on the surfaces were eliminated from the calculation).

the total number of contrast peaks between different images. However, the deviation of contrast peaks in an image is a reliable evidence to reveal the distribution of microstructural changes. Fig. 17 illustrates the distributions of contrast peaks in STEM images of the indent plane and edge (Fig. 16 (b) and (d)), respectively, and the graph shows the calculated densities of contrast peaks for each region. For the indent plane, the outside region of the indent (region a2) exhibited a ~14% higher density than beneath the indent (region a1). For the indent edge, the outside region of the indent (region b1) exhibited a ~41% lower density of contrast peaks than beneath the indent (region b2). This result suggests that the indent plane shows significant deformation and microstructural changes (monoclinic variants in this case), whereas the indent edge does not. This result agrees with that surface pileups observed at the indent edges were smaller than indent planes (Figs. 9 and 10) and that the monoclinic volume ratios at the indent edges were lower than those of the indent planes, as shown in Fig. 14 (~17% lower in single indentation, ~29% lower in multi-cyclic indentation on the unmachined surface).

To verify the expansion of the affected regions by multi-cyclic indentations, the sizes of the indentation-affected regions on the unmachined surface were measured. The depth of the grain-refinement was measured from STEM images and the width of phase transformation regions was measured by Raman mapping. Raman mapping was done in 500 nm intervals from the indent planes toward outside. The spots

Table 4
Sizes of the indentation-affected regions of the unmachined surface.

	Depth of residual indent [μm]	Length of indent side [μm]	Depth of grain refinement region [μm]	Width of phase transformation region [μm]
Single	0.97	9.95	0.41	5.83
Multi-cyclic	1.09	10.78	0.43	6.23
Difference	0.12	0.83	0.02	0.40

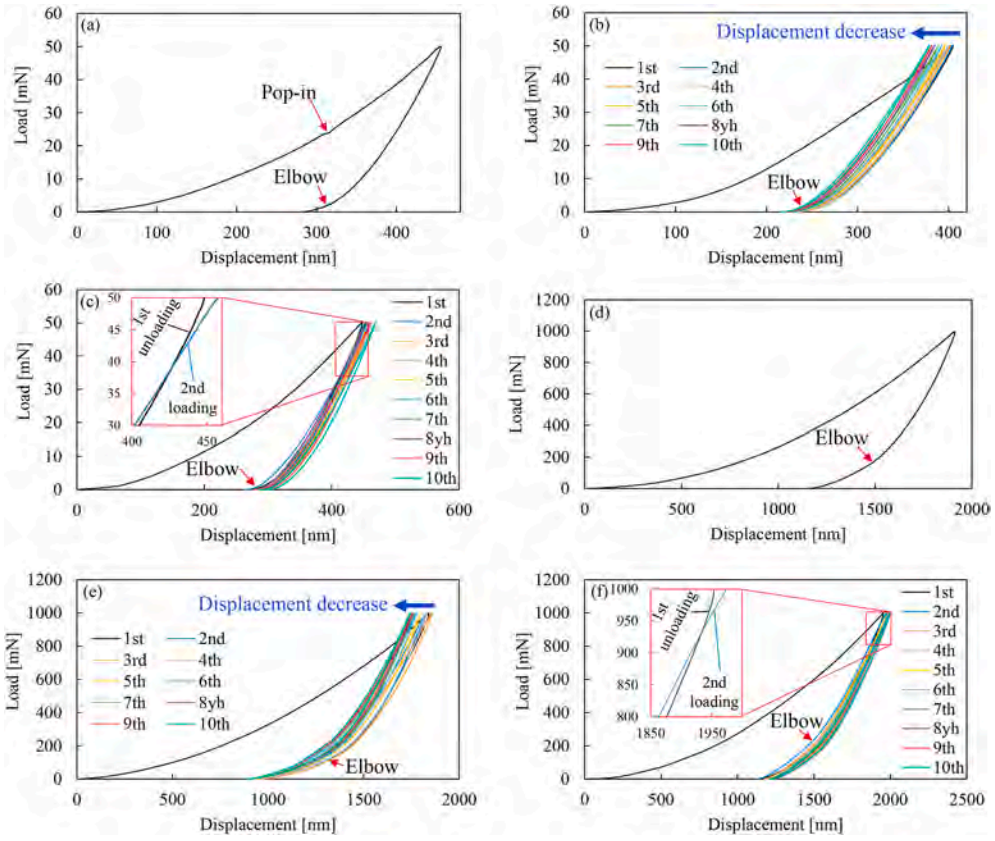

Fig. 18. Load-displacement curves for the unmachined surface (in the enlarged graphs in (c) and (f), only the 1st unloading and 2nd loading curves are illustrated for visibility of their intersection): (a) 50 mN, single; (b) 50 mN, multi (displacement decrease at the maximum load); (c) 50 mN, multi (displacement increase at the maximum load); (d) 1000 mN, single; (e) 1000 mN, multi (displacement decrease at the maximum load); (f) 1000 mN, multi (displacement increase at the maximum load).

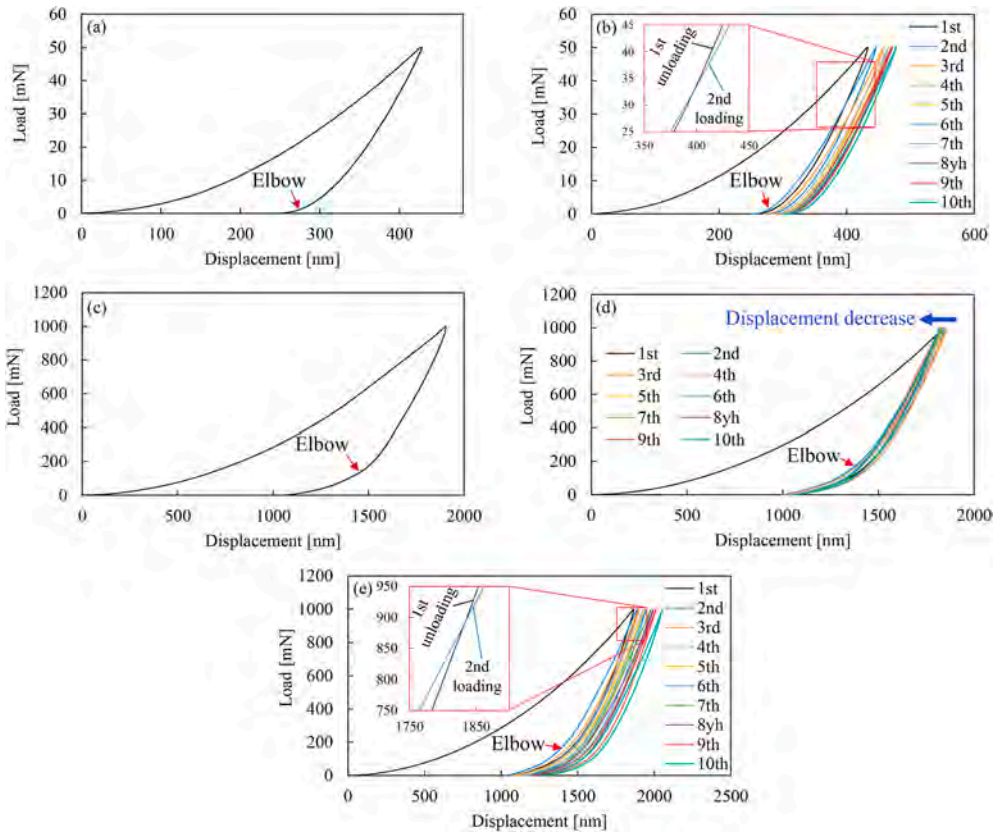

Fig. 19. Load-displacement curves for the diamond-turned surface (in the enlarged graphs in (b) and (e), only the 1st unloading and 2nd loading curves are illustrated for visibility of their intersection): (a) 50 mN, single; (b) 50 mN, multi (displacement increase at the maximum load); (c) 1000 mN, single; (d) 1000 mN, multi (displacement decrease at the maximum load); (e) 1000 mN, multi (displacement increase at the maximum load).

where the monoclinic volume ratio became less than 0.05 (the maximum value on the initial surface) were regarded as the end of phase transformation regions. The results are shown in Table 4. In multi-cyclic indentation, the expansion of the phase transformation regions in the surface direction was more significant than the increase of refined grains in the depth direction. Namely, in multi-cyclic indentation of YSZ, the effect of loading/unloading in the surface direction is stronger than that in the depth direction, which is distinctly different from those of other materials like silicon [48,49].

3.6. Load-displacement characteritics

For explaining the temporal evolution of the aforementioned phase transformation behaviors, load-displacement characteristics were analyzed from load-displacement curves. Fig. 18 and Fig. 19 show the load-displacement curves of single and multi-cyclic indentations on unmachined and diamond-turned surfaces, respectively. As shown in Fig. 18 (a), pop-in events appeared on some loading curves of single indentations at a maximum load of 50 mN. The pop-in might have been caused by sudden slips at indenter-specimen interfaces rather than by phase transformation, because normally the t-m phase transformation causes volume expansion, not volume reduction.

On the unloading curves, sudden slope transitions, so-called elbows, were observed as indicated in Figs. 18 and 19. This phenomenon is a result of phase transformation with volume expansion for some other materials such as silicon [50,51]. In this study, the elbow indicates the occurrence of t-m phase transformation with volume expansion. In loading processes, shear stress was accumulated, but compression was also applied which suppressed t-m phase transformation [43]. However, in unloading processes, as the compression was removed gradually, t-m phase transformation was activated. The phase transformation region expanded from the outer region, where the shear stress was dominant, toward the indent center, where compressive stress still existed. During this process, gradual volume expansion caused the elbows.

After the 2nd cycle in multi-cyclic indentation, the plastic deformation caused by loading, i.e., the gap between the loading and unloading curves, became significantly smaller than that of the 1st cycle, which is a popular phenomenon in multi-cyclic indentation [25,52]. In addition, there are some other characteristic deformation behaviors corresponding to t-m phase transformation on the load-displacement curves. For some multi-cyclic indentations, the displacement at the maximum load on later cycles was smaller than that of 1st cycle, as shown in Fig. 18 (b) and (e), as well as Fig. 19 (d). For some other curves, the displacement at the maximum load gradually increased with cyclic number, but intersections of unloading curves and the subsequent loading curves were observed, as seen in Fig. 18 (c) and (f), as well as Fig. 19 (b) and (e). These phenomena suggest that in addition to elastic recovery, volume expansion caused by phase transformation [43,53] also occurred during unloading. The volume expansion of the material causes changes of residual indent depth among multiple indention cycles. This means that in a machining process, the effective depth of cut and the height of the final finished surface may change among the multiple tool passes, which is an important factor affecting the form accuracy of a workpiece.

3.7. Average contact pressure analysis

In addition to load-displacement curves, average contact pressure (ACP) is also an important factor for investigating the temporal deformation behaviors. Hence, the ACP applied by the indenter was calculated by using the method proposed by Novikov et al. [54], which is widely utilized to monitor the pressure applied on the indented surface during single indentation [51] and multi-cyclic indentations of silicon

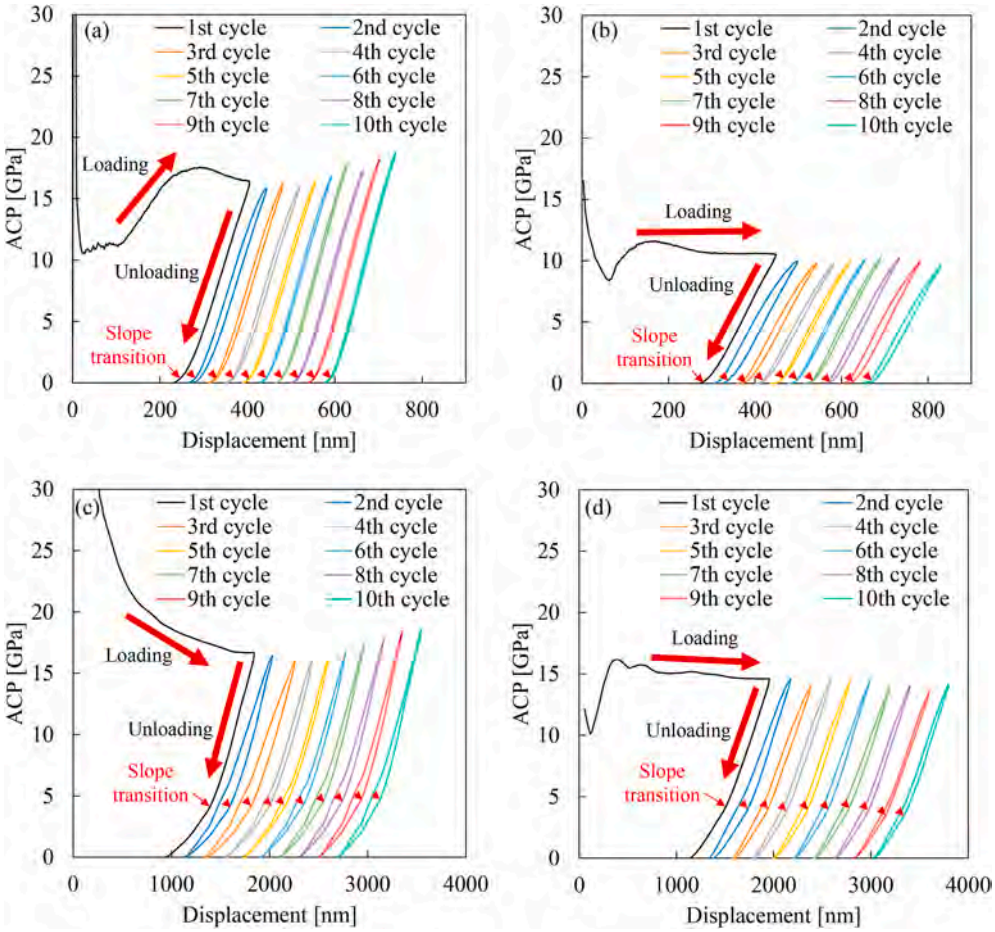

Fig. 20. ACP during multi-cyclic indentation in Fig. 18 on the unmachined surface (40 nm shift for 50 mN are inserted between each cycle, as well as 200 nm shift for 1000 mN); (a) 50 mN with displacement decrease (Fig. 18 (b)); (b) 50 mN with displacement increase (Fig. 18 (c)); (c) 1000 mN with displacement decrease (Fig. 18 (e)); (d) 1000 mN with displacement increase (Fig. 18 (f)).

[25], germanium [28], and gallium arsenide [29]. In this method, elastic deflection of the indented surface is assumed to be proportional to the square root of the applied load. Fig. 20 and Fig. 21 illustrate the calculated ACP during multi-cyclic indentations given in Figs. 18 and 19, respectively. In the graphs, slope transitions of the curves were observed on unloading. After the transition points, the displacement decrease became faster. The transitions corresponded to the elbows on the load-displacement curves, indicating t-m phase transformation. Although plastic deformation, namely, a gap between loading and unloading curves, is observed in the 2nd-10th cycles, the gap is decreased after the slope transition. This means that volume expansion by t-m phase transformation contributed to decreasing the gap in each cycle. It is also shown that the slope transitions occurred almost at the same ACP for all the cycles, which demonstrates the incremental occurrence of t-m phase transformation during multi-cyclic indentation. The incremental t-m phase transformation during multi-cyclic indentation resulted in the extensive monoclinic variants around the indent plane as observed in Fig. 16 (b).

Comparing the cases of 50 mN and 1000 mN in Figs. 20 and 21, the slope transitions, where t-m phase transformation started, occurred at a lower ACP for 50 mN than those for 1000 mN. This is because of different sizes of stressed regions around the indents. Because the stressed region around the indent was small at a maximum load of 50 mN, t-m phase transformation was restricted to a small region near the indent. As a result, compressive stress had to be well released to start t-m phase transformation, thus t-m phase transformation started at a low ACP. On the other hand, the stressed region around the indent was larger at a maximum load of 1000 mN. Therefore, t-m phase transformation could occur even at a more distant region where compressive stress was small and start after a slight release of compression at the early part of unloading.

3.8. Mechanism of subsurface microstructural changes

Based on the experimental results, a distribution model for subsurface microstructural changes of YSZ during multi-cyclic indentation was proposed as Fig. 22. At the 1st cycle, as loading progresses, the stressed region expands (Fig. 22 (a)). The compressive stress inhibits the t-m phase transformation, especially at the indent center. In the unloading process, when the compressive stress is gradually removed, the shear stress accumulated on loading triggers the t-m phase transformation (Fig. 22 (b)). The t-m phase transformation occurs preferentially in the surrounding regions of indent planes and gradually expands toward the indent center during an unloading process. In this process, an elbow appears on the unloading curve because of the phase transformation inducing volume expansion. Although t-m phase transformation occurs in refined grains, the amount is smaller than that around the indent planes (Fig. 22 (c)). In the later cycles, the t-m phase transformation region expands incrementally with presence of repetitive elbows (Fig. 22 (d)–(f)). Finally, extensive monoclinic variants are formed around the indent planes (Fig. 22 (g)), which results in a significant increase of the monoclinic volume ratios.

The present study, for the first time, provided the direct evidence of the microstructural changes on both unmachined and diamond-turned surfaces during multi-cyclic indentations. We found that multi-cyclic indentation did not change constituent phases in YSZ like in silicon

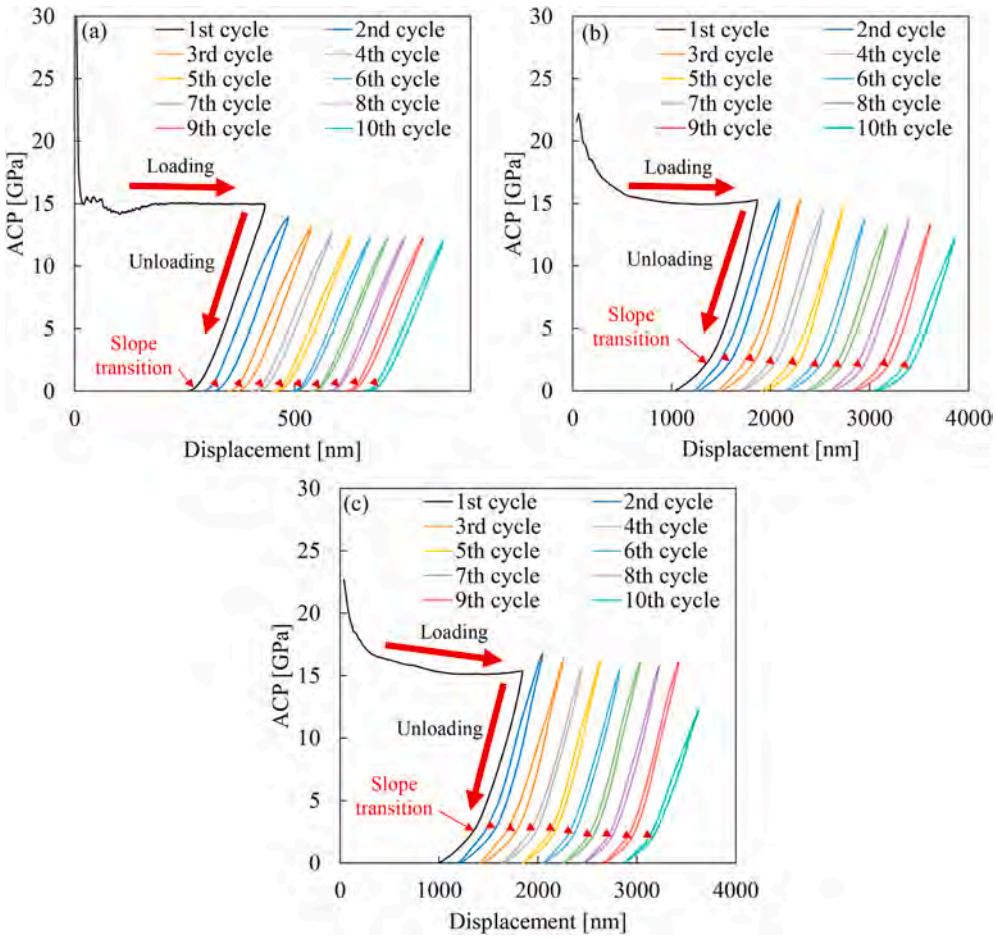

Fig. 21. ACP during multi-cyclic indentation in Fig. 19 on the diamond-turned surface (40 nm shift for 50 mN are inserted between each cycle, as well as 200 nm shift for 1000 mN); (a) 50 mN with displacement increase (Fig. 19 (b)); (b) 1000 mN with displacement decrease (Fig. 19 (d)); (c) 1000 mN with displacement increase (Fig. 19 (e)).

[25]. In addition, the extensive monoclinic variants propagated near the free surface outside the indent plane rather than beneath the indenter. At the indent center, grain refinement was dominant. This is distinctly different from that of silicon [48,49]. Such findings of subsurface behaviors provide important insights into nanoscale material deformation behaviors and subsurface damage formation mechanism of YSZ.

Moreover, in the present study, a rapid displacement decrease on "unloading" due to t-m phase transformation was firstly recognized via smaller displacement on later cycles or intersections of unloading and subsequent loading curves. As only the "loading" process has been focused in previous studies, such unloading behaviors corresponding to t-m phase transformation could not be identified before. Therefore, the present study revealed new aspects of t-m phase transformation behaviors in multi-cyclic indentation of YSZ, which is important for clarifying the cyclic load effect in material deformation and phase transformation.

The above-revealed mechanism of subsurface microstructural changes under multi-cyclic nanoindentation is helpful to understand the behaviors of YSZ polycrystals under cyclic loading/unloading conditions for various precision machining processes involving multiple tool-workpiece interactions. In addition, this study demonstrated that a diamond-turned surface exhibited a similar tendency of subsurface t-m phase transformation behaviors but distinctly different surface morphology in the regard of cracking and spalling.

4. Conclusions

Multi-cyclic nanoindentation tests were performed on yttria stabilized zirconia (YSZ) polycrystals to clarify the microstructural changes due to repetitive loading/unloading. The tetragonal-to-monoclinic (t-m) phase transformation behaviors were analyzed by Raman spectroscopy. Deformation/fracture behaviors were examined by SEM, AFM, and STEM observations, as well as mechanical responses investigated by load-displacement curve analysis. As a result, the following conclusions were obtained:

(1) In multi-cyclic indentation, surface plastic extrusion occurs inside the indents due to cyclic shear deformation at the interface of the indenter and the workpiece material, which indicates that surface roughening may occur in a machining process with multiple tool passes.
(2) The diamond-turned surface exhibits ~1.0 GPa higher microhardness than the unmachined surface at a maximum load of 50 mN, due to the presence of cutting-induced grain-refinement layer, while shows ~1.1 GPa lower hardness at a maximum load of 1000 mN, due to the indentation-induced cracking of the grain-refinement layer. Multi-cyclic nanoindentation on the diamond-turned surface induces spalling of the grain-refinement layer from the bulk along their boundaries.
(3) The monoclinic volume ratio of the diamond-turned surface is ~5% lower at the indent plane, 16–25% lower at the edge than that of the unmachined surface. The cutting-induced grain refinement and residual compressive stress may suppress the t-m phase transformation. In addition, the indentation-induced fractures of the grain-refinement layer may release the shear stress which is necessary to cause phase transformation.

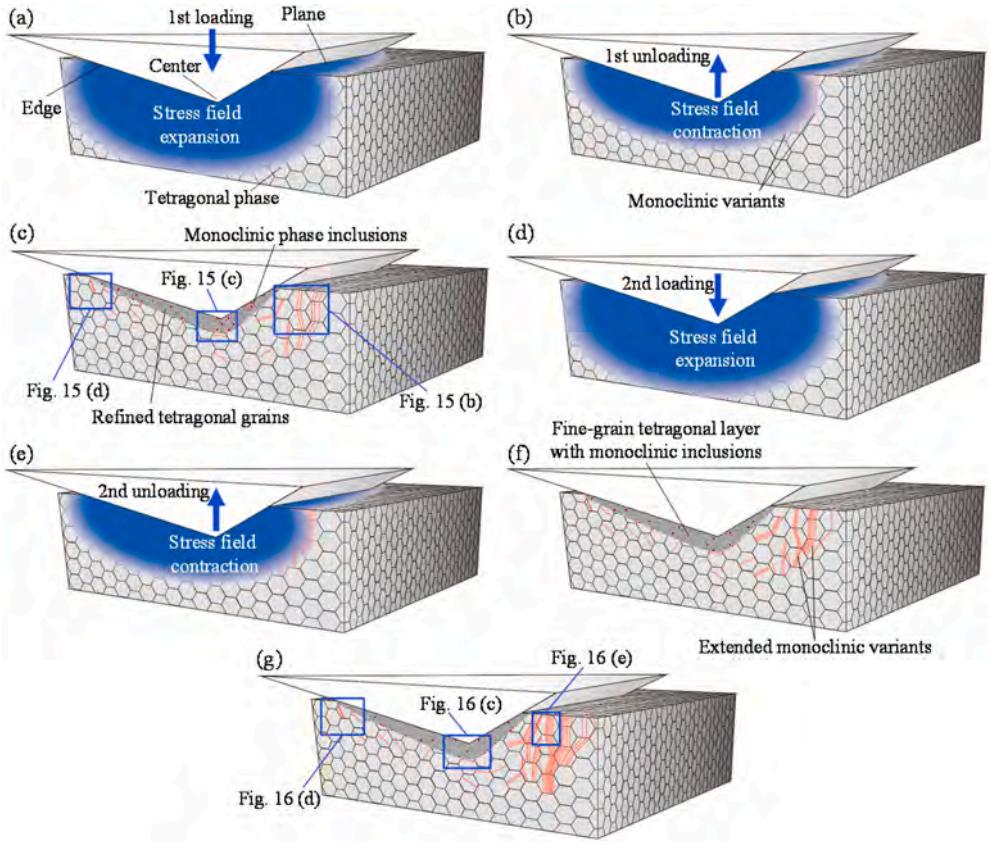

Fig. 22. Schematic model for subsurface microstructural changes of YSZ during multi-cyclic indentation: (a) during 1st loading; (b) during 1st unloading; (c) after 1st unloading; (d) during 2nd loading; (e) during 2nd unloading; (f) after 2nd unloading; (g) after multi-cyclic indentation.

(4) The indent planes exhibit the highest monoclinic volume ratios, whereas the indent centers show the lowest ones. The indent edges present a medium level of t-m phase transformation. Beneath the indent centers, grain refinement is dominant and t-m phase transformation is suppressed due to high compressive stress. This subsurface microstructural change pattern is distinctly different from that of other materials like silicon.
(5) Compared to single indentation, multi-cyclic indentation increases the monoclinic volume ratios by ~13% at the indent plane of the unmachined surface due to the incremental extension of shear zone. The cyclic loading effect results in extensive monoclinic variants outside the indent and higher pileups than those of single indentation. In multi-cyclic indentation, the expansion of the phase transformation region in the surface direction is more significant than that in the depth direction.
(6) A rapid displacement decrease on unloading due to t-m phase transformation was firstly recognized via smaller displacement on later cycles or intersections of unloading and subsequent loading curves in multi-cyclic indentation. The phase transformation-induced volume expansion of the material causes changes of residual indent depth and surface height among multiple indention cycles. This finding indicates that effective depth of cut may change unstably in nanoscale mechanical machining processes with multiple tool passes.

This study revealed the historical effects in the microstructural changes of YSZ under multiple cyclic loading/unloading, which provides useful information for analyzing the fundamental mechanisms and surface integrity for various micro/nanoscale machining processes with multiple tool passes and repetitive tool-workpiece interactions. The findings from this study also help to clarify the subsurface damage and wear mechanisms and their evolutions of YSZ under cyclic loads in dental and biomedical applications. The results are also cultivable for investigating other brittle solids with similar crystalline structures and mechanical properties.

CRediT authorship contribution statement

Koji Kosai: Data curation, Investigation, Writing - original draft. **Jiwang Yan:** Conceptualization, Methodology, Supervision, Writing - review & editing.

Declaration of competing interest

The authors declare that they have no known competing financial interests or personal relationships that could have appeared to influence the work reported in this paper.

Acknowledgements

This work has been partially supported by Keio University Doctorate Student Grant-in-Aid Program. Thanks are extended to Mr. Takumi Okuuchi of the Laboratory for Precision Machining and Nano Processing, Keio University for his assistance in sample preparation by diamond turning for this study.

References

[1] E.P. Butler, Transformation-toughened zirconia ceramics, Mater. Sci. Technol. 1 (1985) 417–432, https://doi.org/10.1179/mst.1985.1.6.417.
[2] C. Piconi, G. Maccauro, Zirconia as a ceramic biomaterial, Biomaterials 20 (1999) 1–25, https://doi.org/10.1016/S0142-9612(98)00010-6.
[3] X. Zhao, D. Vanderbilt, Phonons and lattice dielectric properties of zirconia, Phys. Rev. B Condens. Matter 65 (2002) 1–10, https://doi.org/10.1103/PhysRevB.65.075105.

[4] R.C. Garvie, R.H. Hannink, R.T. Pascoe, Ceramic steel? Nature 258 (1975) 703–704, https://doi.org/10.1038/258703a0.
[5] J. Yan, T. Okuuchi, Chip morphology and surface integrity in ultraprecision cutting of yttria-stabilized tetragonal zirconia polycrystal, CIRP Ann (2019) 1–4, https://doi.org/10.1016/j.cirp.2019.04.050.
[6] I.-W. Chen, P.E.R. Morel, Implications of transformation plasticity in ZrO2-containing ceramics: I, shear and dilatation effects, J. Am. Ceram. Soc. 69 (1986) 181–189, https://doi.org/10.1111/j.1151-2916.1986.tb07403.x.
[7] M. Mamivand, M. Asle Zaeem, H. El Kadiri, Phase field modeling of stress-induced tetragonal-to-monoclinic transformation in zirconia and its effect on transformation toughening, Acta Mater. 64 (2014) 208–219, https://doi.org/10.1016/j.actamat.2013.10.031.
[8] R.H.J. Hannink, P.M. Kelly, B.C. Muddle, Transformation toughening in zirconia-containing ceramics, J. Am. Ceram. Soc. 83 (2000) 461–487. https://ceramics-onlinelibrary-wiley-com.kras1.lib.keio.ac.jp/doi/abs/10.1111/j.1151-2916.2000.tb01221.x.
[9] J.A. Muñoz-Tabares, E. Jiménez-Piqué, M. Anglada, Subsurface evaluation of hydrothermal degradation of zirconia, Acta Mater. 59 (2011) 473–484, https://doi.org/10.1016/j.actamat.2010.09.047.
[10] Y. Gaillard, M. Anglada, E. Jiménez-Piqué, Nanoindentation of yttria-doped zirconia: effect of crystallographic structure on deformation mechanisms, J. Mater. Res. 24 (2009) 719–727, https://doi.org/10.1557/jmr.2009.0091.
[11] A. Paul, B. Vaidhyanathan, J. Binner, Micro-Raman spectroscopy of indentation induced phase transformation in nanozirconia ceramics, Adv. Appl. Ceram. 110 (2011) 114–119, https://doi.org/10.1179/1743676110Y.0000000016.
[12] M.J. Reece, P.L. Tetlow, C. Galiotis, Phase transformation around indentations in zirconia, J. Mater. Sci. Lett. 11 (1992) 575–577, https://doi.org/10.1007/BF00728613.
[13] A. Maerten, P. Zaslansky, C. Mochales, T. Traykova, W.D. Mueller, P. Fratzl, C. Fleck, Characterizing the transformation near indents and cracks in clinically used dental yttria-stabilized zirconium oxide constructs, Dent. Mater. 29 (2013) 241–251, https://doi.org/10.1016/j.dental.2012.10.008.
[14] J.A. Muñoz-Tabares, E. Jiménez-Piqué, J. Reyes-Gasga, M. Anglada, Microstructural changes in 3Y-TZP induced by scratching and indentation, J. Eur. Ceram. Soc. 32 (2012) 3919–3927, https://doi.org/10.1016/j.jeurceramsoc.2012.02.026.
[15] J.A. Muñoz-Tabares, E. Jiménez-Piqué, J. Reyes-Gasga, M. Anglada, Microstructural changes in ground 3Y-TZP and their effect on mechanical properties, Acta Mater. 59 (2011) 6670–6683, https://doi.org/10.1016/j.actamat.2011.07.024.
[16] E. Liu, G. Xiao, W. Jia, X. Shu, X. Yang, Y. Wang, Strain-induced phase transformation behavior of stabilized zirconia ceramics studied via nanoindentation, J. Mech. Behav. Biomed. Mater. 75 (2017) 14–19, https://doi.org/10.1016/j.jmbbm.2017.07.006.
[17] T. Kosmac, C. Oblak, P. Jevnikar, N. Funduk, L. Marion, The effect of surface grinding and sandblasting on flexural strength and reliability of Y-TZP zirconia ceramic, Dent. Mater. 15 (1999) 426–433, https://doi.org/10.1016/S0109-5641(99)00070-6.
[18] T. Kizaki, K. Harada, M. Mitsuishi, Efficient and precise cutting of zirconia ceramics using heated cutting tool, CIRP Ann. - Manuf. Technol. 63 (2014) 105–108, https://doi.org/10.1016/j.cirp.2014.03.073.
[19] J. Yan, T. Asami, H. Harada, T. Kuriyagawa, Fundamental investigation of subsurface damage in single crystalline silicon caused by diamond machining, Precis. Eng. 33 (2009) 378–386, https://doi.org/10.1016/j.precisioneng.2008.10.008.
[20] H. Tang, Z.H. Deng, Y.S. Guo, J. Qian, D. Reynaerts, Depth-of-cut errors in ELID surface grinding of zirconia-based ceramics, Int. J. Mach. Tool Manufact. 88 (2015) 34–41, https://doi.org/10.1016/j.ijmachtools.2014.08.003.
[21] T.G. Bifano, T.A. Dow, R.O. Scattergood, Ductile-Regime grinding: a new technology for machining brittle materials, J. Manuf. Sci. Eng. Trans. ASME. 113 (1991) 184–189, https://doi.org/10.1115/1.2899676.
[22] M. Yang, C. Li, Y. Zhang, D. Jia, X. Zhang, Y. Hou, R. Li, J. Wang, Maximum undeformed equivalent chip thickness for ductile-brittle transition of zirconia ceramics under different lubrication conditions, Int. J. Mach. Tool Manufact. 122 (2017) 55–65, https://doi.org/10.1016/j.ijmachtools.2017.06.003.
[23] C. Zhang, J. Zhang, P. Feng, Mathematical model for cutting force in rotary ultrasonic face milling of brittle materials, Int. J. Adv. Manuf. Technol. 69 (2013) 161–170, https://doi.org/10.1007/s00170-013-5004-z.
[24] X. Xiao, K. Zheng, W. Liao, H. Meng, Study on cutting force model in ultrasonic vibration assisted side grinding of zirconia ceramics, Int. J. Mach. Tool Manufact. 104 (2016) 58–67, https://doi.org/10.1016/j.ijmachtools.2016.01.004.
[25] H. Huang, J. Yan, On the mechanism of secondary pop-out in cyclic nanoindentation of single-crystal silicon, J. Mater. Res. 30 (2015) 1861–1868, https://doi.org/10.1557/jmr.2015.120.
[26] N. Fujisawa, S. Ruffell, J.E. Bradby, J.S. Williams, B. Haberl, O.L. Warren, Understanding pressure-induced phase-transformation behavior in silicon through in situ electrical probing under cyclic loading conditions, J. Appl. Phys. 105 (2009) 1–4, https://doi.org/10.1063/1.3130154.
[27] K. Kosai, H. Huang, J. Yan, Comparative study of phase transformation in single-crystal germanium during single and cyclic nanoindentation, Crystals 7 (2017) 333, https://doi.org/10.3390/cryst7110333.
[28] K. Kosai, J. Yan, Direct observations of multi-cyclic nanoindentation-induced phase transformations in single-crystal Ge, Mater. Res. Express 6 (2019) 75065, https://doi.org/10.1088/2053-1591/ab1986.
[29] Y.G. Gogotsi, V. Domnich, S.N. Dub, A. Kailer, K.G. Nickel, Cyclic nanoindentation and Raman microspectroscopy study of phase transformations in semiconductors, J. Mater. Res. 15 (2000) 871–879, https://doi.org/10.1557/JMR.2000.0124.
[30] S. Deldar, I.A. Alhafez, M. Smaga, T. Beck, H.M. Urbassek, Cyclic indentation of iron: a comparison of experimental and atomistic simulations, Metals 9 (2019), https://doi.org/10.3390/met9050541.
[31] Y.Y. Cui, Y.F. Jia, F.Z. Xuan, Micro-deformation evolutions of the constituent phases in duplex stainless steel during cyclic nanoindentation, Sci. Rep. 8 (2018) 1–10, https://doi.org/10.1038/s41598-018-24589-4.
[32] F. Guiberteau, N.P. Padture, H. Cai, B.R. Lawn, Indentation fatigue, Philos. Mag. A Phys. Condens. Matter, Struct. Defects Mech. Prop. 68 (1993) 1003–1016, https://doi.org/10.1080/01418619308219382.
[33] K. Momma, F. Izumi, VESTA 3 for three-dimensional visualization of crystal, volumetric and morphology data, J. Appl. Crystallogr. 44 (2011) 1272–1276, https://doi.org/10.1107/S0021889811038970.
[34] J.A. Muñoz Tabares, M.J. Anglada, Quantitative analysis of monoclinic phase in 3Y-TZP by Raman spectroscopy, J. Am. Ceram. Soc. 93 (2010) 1790–1795, https://doi.org/10.1111/j.1551-2916.2010.03635.x.
[35] S. Guicciardi, T. Shimozono, G. Pezzotti, Nanoindentation characterization of sub-micrometric Y-TZP ceramics, Adv. Eng. Mater. 8 (2006) 994–997, https://doi.org/10.1002/adem.200600148.
[36] B.A. Cottom, M.J. Mayo, Fracture toughness of nanocrystalline ZrO2-3mol% y2o3 determined by vickers indentation, Scripta Mater. 34 (1996) 809–814, https://doi.org/10.1016/1359-6462(95)00587-0.
[37] S. Bueno, C. Baudin, Instrumented Vickers microindentation of alumina-based materials, J. Mater. Res. 21 (2006) 161–173, https://doi.org/10.1557/jmr.2006.0007.
[38] P. Murali, U. Ramamurty, Embrittlement of a bulk metallic glass due to sub-Tg annealing, Acta Mater. 53 (2005) 1467–1478, https://doi.org/10.1016/j.actamat.2004.11.040.
[39] H. Huang, J. Yan, Investigating shear band interaction in metallic glasses by adjacent nanoindentation, Mater. Sci. Eng. 704 (2017) 375–385, https://doi.org/10.1016/j.msea.2017.08.040.
[40] W. Huang, J. Yan, Surface formation mechanism in ultraprecision diamond turning of coarse-grained polycrystalline ZnSe, Int. J. Mach. Tool Manufact. 153 (2020) 103554, https://doi.org/10.1016/j.ijmachtools.2020.103554.
[41] H. Huang, Y.C. Liu, Experimental investigations of machining characteristics and removal mechanisms of advanced ceramics in high speed deep grinding, Int. J. Mach. Tool Manufact. 43 (2003) 811–823, https://doi.org/10.1016/S0890-6955(03)00050-6.
[42] J. Wang, P. Feng, J. Zhang, C. Zhang, Z. Pei, Modeling the dependency of edge chipping size on the material properties and cutting force for rotary ultrasonic drilling of brittle materials, Int. J. Mach. Tool Manufact. 101 (2016) 18–27, https://doi.org/10.1016/j.ijmachtools.2015.10.005.
[43] F.F. Lange, Transformation toughening - Part 1 Size effects associated with the thermodynamics of constrained transformations, J. Mater. Sci. 17 (1982) 225–234, https://doi.org/10.1007/BF00809057.
[44] S. Huang, J.G.P. Binner, B. Vaidhyanathan, R.I. Todd, Quantitative analysis of the residual stress and dislocation density distributions around indentations in alumina and zirconia toughened alumina (ZTA) ceramics, J. Eur. Ceram. Soc. 34 (2014) 753–763, https://doi.org/10.1016/j.jeurceramsoc.2013.09.021.
[45] A.E. Giannakopoulos, P.L. Larsson, Analysis of pyramid indentation of pressure-sensitive hard metals and ceramics, Mech. Mater. 25 (1997) 1–35, https://doi.org/10.1016/S0167-6636(96)00051-8.
[46] W. Zhang, G. Subhash, Finite element analysis of interacting Vickers indentations on brittle materials, Acta Mater. 49 (2001) 2961–2974, https://doi.org/10.1016/S1359-6454(01)00198-7.
[47] K. Edalati, S. Toh, Y. Ikoma, Z. Horita, Plastic deformation and allotropic phase transformations in zirconia ceramics during high-pressure torsion, Scripta Mater. 65 (2011) 974–977, https://doi.org/10.1016/j.scriptamat.2011.08.024.
[48] S. Ruffell, J.E. Bradby, J.S. Williams, High pressure crystalline phase formation during nanoindentation: amorphous versus crystalline silicon, Appl. Phys. Lett. 89 (2006), 091919, https://doi.org/10.1063/1.2339039.
[49] J. Il Jang, M.J. Lance, S. Wen, T.Y. Tsui, G.M. Pharr, Indentation-induced phase transformations in silicon: influences of load, rate and indenter angle on the transformation behavior, Acta Mater. 53 (2005) 1759–1770, https://doi.org/10.1016/j.actamat.2004.12.025.
[50] V. Domnich, Y. Gogotsi, S. Dub, Effect of phase transformations on the shape of the unloading curve in the nanoindentation of silicon, Appl. Phys. Lett. 76 (2000) 2214–2216, https://doi.org/10.1063/1.126300.
[51] T. Juliano, Y. Gogotsi, V. Domnich, Effect of indentation unloading conditions on phase transformation induced events in silicon, J. Mater. Res. 18 (2003) 1192–1201, https://doi.org/10.1557/JMR.2003.0164.
[52] H. Huang, J. Yan, New insights into phase transformations in single crystal silicon by controlled cyclic nanoindentation, Scripta Mater. 102 (2015) 35–38, https://doi.org/10.1016/j.scriptamat.2015.02.008.
[53] S. Deville, J. Chevalier, H. El Attaoui, Atomic force microscopy study and qualitative analysis of martensite relief in zirconia, J. Am. Ceram. Soc. 88 (2005) 1261–1267, https://doi.org/10.1111/j.1551-2916.2005.00174.x.
[54] N.V. Novikov, S.N. Dub, Y.V. Milman, I.V. Gridneva, S.I. Chugunova, Application of nanoindentation method to study a semiconductor-metal phase transformation in silicon, J. Superhard Mater. 18 (1996) 32.